# EFFECTIVENESS METHOD FOR HEAT AND MASS TRANSFER IN MEMBRANE HUMIDIFIERS

by

DAVID ERWIN KADYLAK

B.A.Sc., The University of Waterloo, 2006

A THESIS SUBMITTED IN PARTIAL FULFILLMENT OF
THE REQUIREMENTS FOR THE DEGREE OF

MASTER OF APPLIED SCIENCE

in

The Faculty of Graduate Studies

(Mechanical Engineering)

THE UNIVERSITY OF BRITISH COLUMBIA

(Vancouver)

April 2009

## ABSTRACT

A thermodynamic model for use in predicting heat and water transfer across a membrane in a membrane humidifier was created that could take into account fuel cell operating conditions. Experiments were conducted to obtain the necessary information to make the model complete, and also to validate its use over a range of temperatures and flow rates.

The latent effectiveness and latent number of transfer units ($\varepsilon$-NTU) method for mass transfer in membrane humidity exchangers was applied to PEMFC membrane humidifiers to comprise the heat and mass transfer thermodynamic model. Two limitations that cause deviations in the theoretical outlet conditions previously reported were discovered: 1. using a constant enthalpy of vaporization derived from the reference temperature in the Clausius-Clapeyron equation; and, 2. simplifying the relationship between relative humidity and absolute humidity as linear. In the model presented here, these limitations are alleviated by using an effective mass transfer coefficient $U_{eff}$. The model was created in Mathcad and the constitutive equations are solved iteratively to find the flux of water through the membrane.

The new procedure was applied to three types of membrane and compared to the curves of $\varepsilon_L$ and $NTU_L$ found using Zhang and Niu's method, which is normally applied to energy recovery ventilators (ERVs). For a 70°C isothermal case, a deviation in latent effectiveness predictions was observed of 29% for Type-I membranes, 23% for linear-type membranes, and 46% for Type-III membranes, as compared to the latent effectiveness values obtained with the ERV method.

Experiments were conducted on a commercially available fuel cell humidifier to determine which parameters could be removed from a full-factorial experimental matrix. It was discovered that pressure had a lower effect on water transport than temperature over the practical operating range of fuel cell systems, so pressure effects were neglected throughout the study. The focus of the study was then on the effect of overall temperature. Furthermore, it was determined that water recovery ratio is the best performance metric because it takes into account the water supplied to the humidifier.

Two different membranes were characterized to incorporate into the thermodynamic model. The first, used as a baseline, was a porous polymer membrane with a hydrophilic additive. The second membrane was a competing novel ionic membrane. Both membranes showed similar behavior, with low water uptake profiles at relative humidities less than 80%, and a steep increase in water uptake after 80% relative humidity. The porous membrane exhibited greater maximum sorption than the ionic membrane.

Experiments were conducted with samples of the porous and ionic membrane in a single cell humidifier at isothermal conditions at temperatures of 25°C, 50°C, and 75°C. The ionic membrane showed greater water transfer over the range of laminar flows investigated. The ionic membrane's water recovery was almost unaffected by flow rate; whereas the porous membrane displayed a decrease in water recovery as flow rate increased. Finally, the model was correlated with the experimental data by obtaining a corresponding diffusion coefficient for each membrane over the range of temperatures tested.

**Keywords:** humidifier, membrane, fuel cell, effectiveness, moisture transfer, NTU

# TABLE OF CONTENTS

# LIST OF TABLES

# LIST OF FIGURES

# LIST OF SYMBOLS AND ABBREVIATIONS

| *Symbol* | *Description (units)* |
|---|---|
| $A$ | membrane surface area ($m^2$) |
| $B$ | width of humidifier (m) |
| $C$ | constant parameter for sorption curve equation |
| $c_p$ | specific heat capacity at constant pressure (J $kg^{-1}$ $K^{-1}$) |
| $C_r$ | ratio for heat capacity |
| $d$ | channel depth (m) |
| $D_{AB}$ | mass diffusivity of species A in species B ($m^2$ $s^{-1}$) |
| $D_h$ | hydraulic diameter (m) |
| $D_{wm}$ | diffusivity of water in membrane (kg $m^{-1}$ $s^{-1}$) |
| DPAT | dew point approach temperature |
| $h$ | convective heat transfer coefficient, or conductance (W $m^{-2}$ $K^{-1}$) |
| $H$ | specific enthalpy (J $kg^{-1}$) |
| $h_M$ | convective mass transfer coefficient, or conductance (kg $m^{-2}$ $s^{-1}$) |
| $\Delta h_{vap}$ | heat of vaporization (J $kg^{-1}$) |
| $J$ | water flux (kg $s^{-1}$ $m^{-2}$) |
| $j_H$ | Chilton-Colburn $j$ factor for heat transfer |
| $j_M$ | Chilton-Colburn $j$ factor for mass transfer |
| $k$ | thermal conductivity (W $m^{-1}$ $K^{-1}$) |
| $l$ | length of channel (m) |
| Le | Lewis number |
| $M$ | molar mass; number of plates (levels) in humidifier |
| $\dot{m}$ | mass flow rate (kg $s^{-1}$) |
| $n$ | number of channels in humidifier plate |
| NTU | number of transfer units |
| Nu | Nusselt number |
| $P$ | pressure (Pa) |
| Pe | Peclet number |
| Pr | Prandtl number |
| $q$ | specific humidity (kg water/kg mixture); heat transfer rate (W) |
| $q_{max}$ | maximum possible heat transfer rate (W) |
| $Q$ | volumetric flow rate (SLPM) |
| $R$ | universal gas constant (J $kg^{-1}$ $K^{-1}$) |
| $R^2$ | coefficient of determination for least-squares fit |
| $R_L$ | ratio for mass capacity |
| Re | Reynolds number |
| Sc | Schmidt number |
| Sh | Sherwood number |
| $St_H$ | Stanton number for heat transfer |
| $St_M$ | Stanton number for mass transfer |
| $T$ | temperature (K) |
| $t$ | thickness (m) |
| $U$ | overall heat transfer coefficient (W $m^{-2}$ $K^{-1}$) |
| $U_L$ | overall mass transfer coefficient (kg $m^{-2}$ $s^{-1}$) |
| $U_{eff}$ | effective mass transfer coefficient (kg $m^{-2}$ $s^{-1}$) |
| $w$ | width of channel (m) |
| WRR | water recovery ratio |
| $z$ | direction of membrane thickness (m) |

*Greek symbols*

| | |
|---|---|
| $\alpha$ | thermal diffusivity ($m^2\ s^{-1}$) |
| $\gamma$ | moisture diffusive resistance ($m^2\ s\ kg^{-1}$) |
| $\varepsilon$ | effectiveness [0,1] |
| $\theta$ | water uptake (kg $H_2O$/kg dry membrane) |
| $\theta_{max}$ | maximum water uptake capacity (kg $H_2O$/kg dry membrane) |
| $\mu$ | dynamic viscosity ($kg\ m^{-1}\ s^{-1}$) |
| $\rho$ | density ($kg\ m^{-3}$) |
| $\phi$ | relative humidity |
| $\Phi$ | placeholder variable for potential driving force |
| $\omega$ | absolute humidity (humidity ratio) (kg $H_2O$/kg dry air) |

*Subscripts*

| | |
|---|---|
| *air* | air species |
| *d* | referring to the dry (or sweep) side |
| *di* | dry-side channel inlet |
| *do* | dry-side channel outlet |
| *dp* | dew point, when used with *T* |
| *H* | enthalpy (or total), used with effectiveness |
| $H_2O$ | water |
| *iso* | isothermal conditions |
| *L* | latent or moisture |
| *mem*, *m* | membrane |
| min | minimum |
| *ref* | reference state |
| *sat* | value at saturation |
| *v* | vapor |
| *w* | referring to the wet (or feed) side |
| *wb* | wet bulb, used with temperature *T* |
| *wi* | wet-side channel inlet |
| *wo* | wet-side channel outlet |

*Abbreviations*

| | |
|---|---|
| ERV | Energy Recovery Ventilator |
| HVAC | Heating, Ventilating and Air Conditioning |
| MEA | Membrane Electrode Assembly |
| PEM | Proton Exchange Membrane |
| PEMFC | Proton Exchange Membrane Fuel Cell |
| PFSA | Perfluorosulfonic Acid (i.e., Nafion™) |
| PTFE | Polytetrafluoroethylene (i.e., Teflon™) |
| PVC | Polyvinyl Chloride |

# ACKNOWLEDGEMENTS

First and foremost, I would like to credit Jesus Christ, the Creator, "in whom are hidden all the treasures of wisdom and knowledge" (Holy Bible, Colossians 2:3), who alone bestows all good gifts.

There are many people from whom I benefitted a great deal during the process of arriving at this culminating work. Dr. Walter Mérida was a great supervisor to have, providing the overall direction to the project, guidance in preparing certain sections into becoming manuscripts for journal articles, and making me refine my work to produce an excellent end-result. Thanks also go to Dr. Martin Davy who sat on the review committee.

James Dean, president of dPoint Technologies, was also instrumental in guiding the contribution found in this work. I am grateful that he allowed me to take just over two years to pursue a master's degree while working part time. I acknowledge Chris Goodchild, test engineer at dPoint Technologies, for performing the required testing and collecting the data outlined in the parameter study and performance metric study. Ryan Huizing, dPoint's resident membrane expert, was also of assistance and even edited a draft of this thesis. I want to thank the rest of the dPoint team as well.

Tatyana Soboleva, Simon Fraser University chemical engineering Ph.D. candidate performing research at the National Research Council, was of immense value for taking the time to run the dynamic vapor sorption instrument with samples I provided.

This work is a testament to past fellow graduate student at UBC; Peter Cave's pioneering work in this area of humidifier modeling research in collaboration with dPoint. Part of the work presented in Section 3.4 and Section 3.5 was based on a

collaborative effort involving Peter Cave. He is a good friend and as well provided insightful comments upon proof-reading a draft copy of this thesis. I want to also thank fellow research students with whom I shared an office and many good discussions: Tatiana Romero, Ed McCarthy (who also provided editing services), Saúl Pazos-Knoop, Omar Herrera, and Amir Niroumand.

I would like to acknowledge the Natural Sciences and Engineering Research Council of Canada for financial assistance through their Canada Graduate Scholarship.

*Soli Deo Gloria*

# 1. INTRODUCTION

Reactant humidifiers, making up the water management part of the balance of plant of a fuel cell system, can make up as much as 20% of the balance of plant cost [1]. Technological improvements to reactant humidifiers will help reduce the costs associated with fuel cell systems that are currently making them commercially unviable. A more fundamental understanding of parameter effects on humidifier design will allow improved designs which will lower costs.

## 1.1. WATER MANAGEMENT IN FUEL CELLS

For optimal performance of a proton exchange membrane fuel cell (PEMFC), the membrane electrode assembly (MEA) requires hydration to enable protonic conduction, and the membrane's conductivity depends on water content [2]. While a PEM fuel cell may be operated with dry streams of air and hydrogen, Rajalakshmi *et al.* [3], among other researchers [2,4,5], have shown that the fuel cell power output increases if the reactant streams are properly humidified (Figure 1.1). Furthermore, adequate hydration extends the lifetime of the fuel cell stack [6].

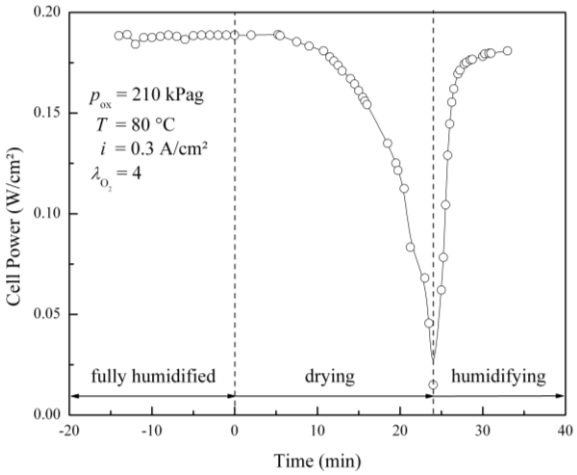


**Figure 1.1:** Effect of reactant stream humidity on PEM fuel cell voltage output; adapted from [5]

A humidifier is required to ensure that the cathode reactant gas, usually air, is hydrated before entering the fuel cell. If the membrane of the MEA operates dry or there is improper hydration, two issues arise: performance degradation and premature failure from pinholes due to changes in mechanical loading [7,8]. As mentioned above, the reaction depends on membrane water content and over time, as more water is removed from the fuel cell through the exhaust, fewer $H^+$ ions will be able to cross the membrane. This leads to a lower reaction rate and compounds the problem because less water is being produced at the cathode side of the reaction. This process acts as a negative feedback system that will continue to intensify until there is no longer any electrochemical reaction. Regarding durability, a typical membrane such as Nafion swells by 10%, and up to 20% or more at high temperatures, going from a dry to a wet state; if there is improper humidification the continual swelling and contracting will induce mechanical stresses leading to membrane failure [9,10]. Operating in drying conditions will also lead to locations in the membrane through which increasing amounts of reactant gas can cross over. Furthermore, running the streams dry will also lead to hot spots due to eliminating the water available as a sink to remove heat from areas of high catalytic activity. This induces localized wear, such as pinholes in the membrane, thereby affecting the long-term use of the MEA [6].

On the other hand, over-humidification may lead to condensation in the fuel cell causing the obstruction or clogging of the flow field paths and prevent delivery of reactant gas. Flooding will be a concern where—offset from the localized area where there is less reaction taking place and so becoming dryer—more of the reaction will be occurring to compensate in the area of the cell which is more hydrated [11].

The humidifier system presented in the model herein will only focus on humidifying the cathode side stream, although the anode side could also be humidified. Figure 1.2 shows the balance of plant for the fuel cell system with a humidifier. It shows how a dry air supply (providing the reactant oxygen) is passed through the humidifier, and is humidified by the wet air exhaust stream coming from the cathode reaction of the fuel cell stack. The membrane is at the heart of the fuel cell humidifier technology, as it allows water to transport from the stream with higher water content ("wet") to the stream with less water content ("dry"), while preventing air from crossing over from one stream to another.

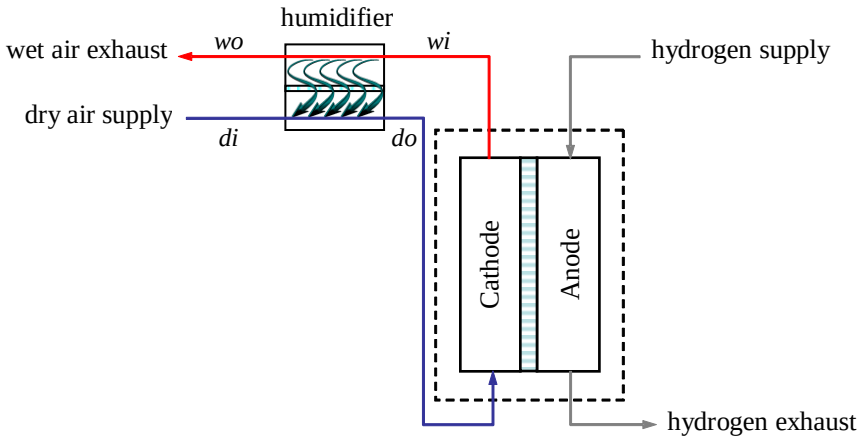


**Figure 1.2:** Balance of plant of humidifier and fuel cell system

Figure 1.2 illustrates a typical implementation of a membrane humidifier at the cathode side of a PEM fuel cell: dry air is pumped from a compressor or blower to the dry inlet of the humidifier. As this dry incoming stream passes over the humidifier membrane it is humidified and heated from the wet inlet stream—exiting from the fuel cell cathode exhaust—by water transport through the membrane. The humidified air then exits the humidifier as the humidified dry outlet stream and enters the fuel cell cathode to

hydrate the MEA. Finally, the humidifier exhaust wet outlet stream exits the humidifier at a lower temperature and humidity than when it entered the humidifier, having supplied moisture and heat to the membrane.

## 1.2. ACTIVE VS. PASSIVE METHODS

An active humidification system is one that requires a physical mechanism for supplying water to the fuel cell stack. Such systems often require onboard stored water to inject water into the reactant stream using a pump, or a complicated cooling system to knock out water through the use of a condenser. One common active method is to provide the necessary water by direct liquid water injection or spraying through an atomizer controlled by a solenoid valve. Furthermore, an electronic control system is required to meter the required amount of water at the different flow rates or fuel cell loadings. While this method provides precise control over humidification, it suffers from the large number of components, making the balance of plant large, heavy and complicated, increasing costs. A danger in employing this method is the potential to run out of liquid water at high fuel cell loadings. An auxiliary benefit to this method of humidification is that it can be used to cool the incoming reactants if necessary through evaporative cooling [2].

Another external active method employs a gas bubbler, where the reactant air is first passed through a liquid water reservoir. It is assumed that the reactant gas leaves saturated at the dew point temperature of the liquid water. This process is also called sparging, and is relatively restricted to laboratory work, with little practical application in on-board fuel cell systems. Other methods include direct internal humidification through

such means as wicks, sponges, or directly injecting liquid water, by modifying the bipolar plates' flow fields [2].

Another active method that is more commonly used than the aforementioned methods uses a rotating cylinder containing a porous desiccant over which the damp exhaust from the fuel cell passes on one side and the reactant passes through another side picking up moisture. Such a device is called an enthalpy wheel, and a major manufacturer for commercial use in fuel cell systems is Emprise Corporation. Several drawbacks to this technology include issues with sealing the moving parts, and the need to power the rotating device, along with control. These issues prohibit the enthalpy wheel from becoming a cost-effective solution.

The most promising type of humidification to use with fuel cells, as indicated by its wider acceptance among fuel cell system integrators, is a passive system where the excess water from the cathode exhaust from the fuel cell reaction is used to humidify the incoming gas. If operating a PEMFC at high pressures, and even at a high temperature, only about half of the exhaust water vapor and liquid is required to maintain the incoming stream hydrated using the product water [2]. Therefore, in a passive system a gas-to-gas humidification system can use the fuel cell exhaust gas stream to humidify the incoming gas stream, while limiting the crossover of air. Minimizing the crossover of air is necessary in order to prevent the depletion of oxygen being supplied to the fuel cell cathode.

A popular passive technology implemented in many fuel cell systems incorporate a shell-and-tube membrane humidifier. This technology is based on the common heat exchanger architecture, except that a hollow fiber membrane allows water to transfer

from a wet stream coming from the fuel cell cathode exhaust to the incoming drier air through the tubular membrane. Perma Pure is a commercial manufacturer of shell-and-tube type membrane humidifiers. A major disadvantage of the available tubular membrane humidifiers is that they are made from an expensive membrane, such as Nafion. Conversely, Nafion membranes have been proven to be a reliable solution to PEMFC humidification, with over 15,000 h of continuous operation.

One other such passive method used to humidify the inlet reactant gas is to use a plate-and-frame type membrane humidifier [12,13]. A conceptual diagram of two layers on either side of the planar humidifier membrane is shown in Figure 1.3. In this case, a membrane separates the "wet" exhaust stream incoming from the fuel cell from the "dry" inlet stream. The membrane allows water to adsorb and pass through, but blocks the cross-over of gas. This type of humidifier has already demonstrated good performance [12]. Possibly the most significant advantage of this type of humidifier is that the membrane, which is usually the most expensive component, can be made from low cost, widely available polymer membranes, such as a high density porous polymer with a hydrophilic additive. Another benefit is that a passive planar membrane humidifier does not require an extra parasitic load, such as to drive a water pump or controller, other than the power required to overcome the low pressure drop through the channels. Other advantages are its light weight, simple design, and having no moving parts, which often lead to sealing issues and early mechanical wear and failure. The design architecture also lends itself well to manufacturing with a continuous automated process. The structure of the design maintains open channel flow fields, where the membrane spacing is maintained, unlike the bundles of hollow fiber tube humidifiers. A prominent supplier of

planar membrane humidifiers is dPoint Technologies, who have also applied the technology to energy recovery ventilators. The plate-and-frame planar membrane humidifier will be the focus of the research presented in this work.

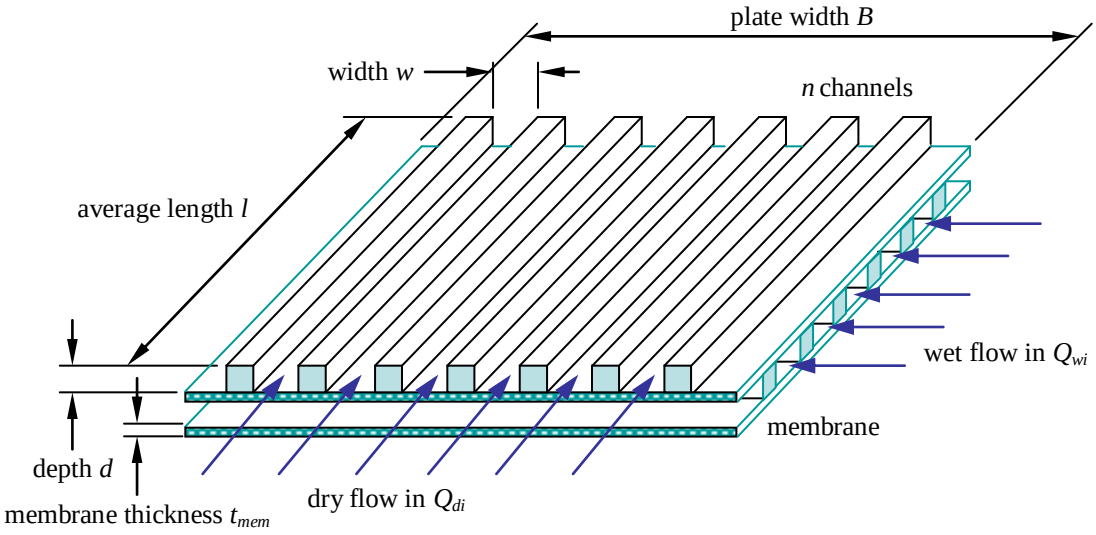


**Figure 1.3:** Schematic of layered humidifier plates in cross-flow arrangement

## 1.3. PERFORMANCE METRICS

The performance of a humidifier, as a device that transfers water and humidifies a dry gas stream, can be gauged by the amount of water it transfers or the amount of humidity it is able to supply.

### 1.3.1. MEASURES BASED ON SUPPLIED HUMIDITY

In the operation of a fuel cell system, the purpose of the humidifier is to supply humidified reactant. Therefore, the humidifier's performance can be analyzed based on the outlet humidity from the dry stream that has been humidified. It has been reported that the PEM fuel cell membrane operates best at a relative humidity close to 100%

[2,14,15], so an appropriate measure would be the outlet relative humidity of the dry stream that supplies the fuel cell. The relative humidity $\phi$ is defined as:

$$\phi = \frac{m_v}{m_{sat}} = \frac{P_v}{P_{sat}} \tag{1}$$

where $P_v$ is the partial vapor pressure of water, and $P_{sat}$ is the saturation vapor pressure. The relative humidity can be considered as describing how far away the state of the gas-water mixture is from the maximum amount of water which occurs at saturation.

Another measure of humidity is the humidity ratio $\omega$, also known as the mixing ratio or absolute humidity, which is a ratio of the mass of water vapor to mass of dry air:

$$\omega = \frac{m_v}{m_{air}} = \frac{M_{H_2O}}{M_{air}} \frac{P_v}{P_{air}} = \frac{0.622\ P_v}{P - P_v} \tag{2}$$

where $M$ is the molecular weight; 0.622 is the molecular weight ratio of water to dry air composition, and the partial pressure of air $P_{air}$ can be found by subtracting the vapor partial pressure $P_v$ from the total pressure $P$.

Similarly, the specific humidity $q$ is a humidity ratio based on the total mass instead of just the mass of dry air:

$$q = \frac{m_v}{m_v + m_{air}} = \frac{\omega}{1 + \omega} \tag{3}$$

Cautions should be taken when using specific humidity in that sometimes it is used interchangeably to mean humidity ratio, and other times absolute humidity is defined on an air volume basis instead of an air mass basis, depending on the source.

A problem arises when using any of the above humidity metrics as a performance measure. A different amount of water to ensure proper hydration will need to be transferred if the operating fuel cell temperature, pressure, or flow rate changes. For

instance, at higher power loads and therefore flow rates, the temperature of the fuel cell will change and the water requirements may change. Therefore, the relative humidity without a dry-bulb temperature, pressure, and flow rate cannot specify the performance of a specific humidifier over a range of operating conditions.

Other outlet humidity measures are wet-bulb temperature $T_{wb}$ and dew point temperature $T_{dp}$, which can be regarded as incorporating humidity and temperature together. The wet-bulb temperature is the temperature of water in the wetted wick of a thermometer that has reached equilibrium with the unsaturated gas that is causing water to evaporate from the wick. At atmospheric pressure, for air and water vapor, the wet-bulb temperature is close to the adiabatic saturation temperature. The dew point temperature is the temperature at which condensation begins to occur when the gas containing water vapor is cooled at constant pressure [16]. It is defined as the water saturation temperature $T_{sat}$ corresponding to the vapor pressure $P_v$:

$$T_{dp} = T_{sat}(P_v) \tag{4}$$

The dew point and wet-bulb temperatures also suffer from the same problem as the other humidity measures, because they fail to correlate straightforwardly to the relative humidity, which will change with actual dry-bulb temperature. The problem is further compounded by the non-linear relation of water vapor pressure with temperature, which may lead to misleading conclusions; this phenomenon will be demonstrated in Section 2.2. The dew point temperature will still be used as a reference to the output of the humidity sensor to be used in the experiments. Using the water vapor pressure $P_v$ as an outlet measure of water presents the same difficulty.

### 1.3.2. ABSOLUTE MEASURES

Absolute measures are metrics that are based on the total amount of water transferred, usually on a mass or molar basis. The total water transfer rate $\dot{m}_{H_2O}$ is simply the rate of water mass transferred across the membrane, such as in units of kg/s. This is a good metric for comparing identical humidifiers over a range of conditions.

To compare different humidifiers over different conditions the water flux $J$ is a better measure, which takes into account the membrane active area $A$ (and hence humidifier size) that the water is transferring through:

$$J = \frac{\dot{m}_{H_2O,do} - \dot{m}_{H_2O,di}}{A} = \frac{\dot{m}_{H_2O}}{A} \tag{5}$$

### 1.3.3. MEASURES BASED ON AVAILABLE HUMIDITY

So far, all the measures to quantify humidifier performance have not addressed how well a humidifier performs compared to how well the device could potentially perform. One such measure that is analogous to the pinch temperature in heat exchanger design is the dew point approach temperature, DPAT. The DPAT is a measure of how close the dry outlet dew point comes to the wet inlet dew point temperature of the humidifier:

$$\text{DPAT} = T_{dp,wi} - T_{dp,do} \tag{6}$$

In a perfect humidifier, the DPAT would reach 0°C. The DPAT is plagued with the same inherent misleading and incomplete information found in using the dew point temperature, because the same DPAT changes significance in terms of water transferred as the conditions change.

Effectiveness measures are common in the heating, ventilating and air conditioning (HVAC) industry. The effectiveness measure follows a common format, with the driving force based on the desired sensible (heat), latent (moisture), or total (enthalpy) effectiveness. For example, total effectiveness is defined from the specific enthalpy *H* as [17]:

$$\varepsilon_H = \frac{(\dot{m} c_p)_d (H_{di} - H_{do})}{(\dot{m} c_p)_{\min} (H_{di} - H_{wi})} \tag{7}$$

The latent effectiveness and water recovery ratio are non-dimensional parameters that describe how effectively a humidifier performs. The latent effectiveness $\varepsilon_L$, commonly used in energy recovery ventilators, is based on the humidity ratio $\omega$:

$$\varepsilon_L = \frac{(\dot{m} c_p)_d (\omega_{di} - \omega_{do})}{(\dot{m} c_p)_{\min} (\omega_{di} - \omega_{wi})} \tag{8}$$

where $c_p(T,\phi)$ is the specific heat of the air and varies with temperature and air composition.

The water recovery ratio, WRR, is a measure that describes how much water is transferred to the dry outlet compared to the amount of water supplied, which would be the maximum amount of water that could be transferred:

$$\text{WRR} = \frac{\dot{m}_{H_2O,do} - \dot{m}_{H_2O,di}}{\dot{m}_{H_2O,wi}} = \frac{(\omega_{do} - \omega_{di})\dot{m}_{air,d}}{\omega_{wi}\dot{m}_{air,w}} \tag{9}$$

If the air flow rates in each of the dry and wet streams are equal, the water recovery ratio reduces to:

$$\text{WRR} \ (\dot{m}_{air,d} = \dot{m}_{air,w}) = \frac{\omega_{do} - \omega_{di}}{\omega_{wi}} \tag{10}$$

The merits of each water transfer measure as a performance metric will be evaluated in Section 2.2 to determine the most appropriate metric to use.

## 1.4. VARIABLES AND PARAMETERS AFFECTING WATER TRANSFER

The variables affecting the performance of humidifiers can be divided into geometric variables, membrane properties, and parameters taken from the flow conditions. The geometry is dictated primarily by the type of humidifier designed. This study will focus on a plate-and-frame heat and humidity exchanger.

### 1.4.1. PLATE GEOMETRY

Table 1.1 presents an overview of the effects that changing the humidifier geometry will have on the variables that contribute to humidifier performance, such as heat transfer, water transfer, and pressure drop.

**Table 1.1:** Dependence of humidifier geometry characteristics on performance

| Geometry | Affects… |
|---|---|
| channel height* | heat and mass transfer coefficients, and fluid velocity through cross sectional area |
| channel width* | heat and mass transfer coefficients, and fluid velocity through cross sectional area |
| channel length* | useable membrane area, and heat transfer coefficient through extended surface area effectiveness |
| number of plates* | flow rate per channel |
| number of channels* | flow rate per channel |
| rib width* | convective heat transfer in the form of effectiveness of extended surface area |
| channel shape* | heat and mass transfer coefficients; incorporated into the model through the hydraulic diameter and assuming a rectangular aspect ratio |

* incorporated into the model

### 1.4.2. MEMBRANE PROPERTIES

As described in Section 2.4.1, the focus of this research is to create a model based on sorption-diffusion theory. This method, as opposed to the permeation method, requires characterizing the membrane and obtaining its sorption curve. Table 1.2 lays out the possible effects membrane properties have on humidifier performance.

**Table 1.2:** Dependence of membrane properties on humidifier performance

| Property | Affects… |
|---|---|
| membrane structure and composition (i.e., porosity, composite layers, etc.)* | whether transport is convective (pressure-driven) or diffusive (concentration-driven); model assumes diffusion-dominated transport, need sorption curves (Section 2.4.1, 0) |
| mechanism to be modeled: | |
| i. membrane diffusivity* | diffusive mass transfer resistance, using Fick's First Law; incorporated into the model (Section 0) |
| ii. membrane permeability | convective mass transfer resistance, using Darcy's Law; assumed to be negligible compared to diffusion driving force for the modes under consideration in the model |
| membrane conductivity* | conductive heat transfer across membrane |
| membrane thickness* | conductive heat transfer and diffusive mass transfer resistance |

* incorporated into the model

### 1.4.3. FLOW CONDITIONS

The flow conditions of the reactant streams are the third class of variables that influence performance. The flow conditions are set by the wet stream supplied by the fuel cell, and the dry stream to be humidified supplied by a blower or compressor. The effects of these streams' flow conditions are summarized in Table 1.3.

**Table 1.3:** Dependence of stream flow conditions on humidifier performance

| Condition | Affects… |
|---|---|
| temperature (fluid/membrane state) or temperature difference (across membrane, to the surroundings)* | relative humidity, thermo-diffusion, heat transfer and heat loss to surroundings, and condensation rate. Also affects membrane and fluid properties. Temperature dependence is incorporated into the model. Temperature effects on heat loss and condensation rate are not incorporated, yet to be investigated |

(continued on next page)

| Condition | Affects… |
|---|---|
| pressure (fluid state) or pressure difference (across membrane)* | convective driving gradient. Capillary water transfer through membrane pores driven by high pressure gradients. Also affects membrane and fluid properties. Pressure dependence incorporated into the model. Effect of pressure through permeability has not been considered (Section 0) |
| pressure drop* | Drop in pressure may have consequences on two-phase flow. This has not been investigated (Section 0). Pressure drop affects state pressure along the channel. Although generally small changes in laminar flow, the effect on fluid properties has been incorporated into the model |
| relative humidity (fluid state) or relative humidity difference (across membrane)* | Relative humidity difference affects water uptake and hence diffusion driving gradient. The relative humidity of the fluid affects fluid properties |
| wet side flow rate or velocity* | residence time and convective heat and mass transfer coefficients |
| dry side flow rate or velocity* | residence time and convective heat and mass transfer coefficients |
| mixture composition* (nitrogen, oxygen, water) | affects fluid properties |
| condensation rate | heat and mass transfer, pressure, and changes flow from single phase to two phase; to be investigated further |
| two phase vs. single phase flow | A consequence of other conditions, but may cause a non-continuous change in transport ability |
| turbulent vs. laminar | A consequence of other conditions, but may cause a non-continuous change in transport ability. Since the vast majority of the flow through the channels will invariably be laminar, the model only considers laminar flow |

* incorporated into the model

## 1.5. THESIS OBJECTIVE

Referring to the recent modeling work of Majsztrik *et al.* [18], Cave and Mérida [12], Chen *et al.* [19], and Huizing *et al.* [13], Park and Oh state "[these models] are difficult to apply in practice because of their complex forms. Hence, a simplified model is necessary and helpful to evaluate humidification… for PEM fuel cell applications" [20]. Although Park and Oh go on to provide a comparable, simple, one-dimensional

thermodynamic model for a liquid-to-gas Nafion membrane humidifier, they fall short of contributing a comprehensive model that may be used in gas-to-gas membrane humidifiers. Their model fails to take into account the convective effects of the flow, and not just the permeability of the selected membrane based on its thickness.

Others have focused on the shell-and-tube design of Nafion membrane humidifiers [19,21,22]. Fuel cell system integrators are seeking to phase out Nafion as a membrane for PEMFC humidification due to its prohibitively high price (at least \$500/$m^2$ [23]), as it is also the usual membrane used in the MEA of the fuel cell stack. The work of Monroe *et al.* is primarily concerned with characterization of membranes, specifically quantifying the interfacial characteristics of Nafion using a simple experimental chamber where the feed gas is circulated and exchanged [24]. Monroe presented a method for obtaining a vaporization-exchange rate coefficient from water vapor permeation experiments for use in his model.

The empirical method applied by Huizing is a simple design parameter that compares the theoretical diffusion time for liquid water from a membrane surface to the residence time of the water vapor in the humidifier [25]. A more detailed thermodynamic model is sought after that will take into account the fundamental physical mechanisms affecting water transport. In that vein, the present work builds on the previous work of Cave [26], but is applicable to various membranes and uses a less complex method.

The effectiveness-number of transfer units ($\varepsilon$-NTU) method is well-known in heat exchanger design for determining the unknown properties of outlet fluid streams, or for setting geometrical and flow parameters to achieve the required composition at the outlets [27,28]. Analyses of heat transfer and mass transfer of water are coupled for attaining the

outlet conditions in an enthalpy exchanger. The formulations of Zhang and Niu of latent effectiveness $\varepsilon_L$ and number of transfer units for moisture transfer $NTU_L$ [29] were extended for use in a membrane heat and humidity plate-and-frame exchanger for use with PEMFC applications. Zhang and Niu, basing their work on the previous work of Simonson and Besant, demonstrated the dependence of performance on membrane type, characterized by its sorption curve (water uptake vs. relative humidity) [29,30].

Table 1.4 lists the related research that is available in the literature, and specifies any comments that relate to the present work. As mentioned earlier, a thermodynamic model that is easy to apply will greatly assist in the design of PEMFC humidifiers. To that end, it is necessary that the model can account for the elevated temperatures, pressures, flow rates, and humidity found in PEMFC operation. It is not certain that Nafion will be the membrane commonly used in commercial fuel cell humidifiers; therefore the model should allow for other membrane types, and not be limited in scope to one architecture, such as shell-and-tube. The column named "Overall approach" in Table 1.4 refers to a model that takes a more general approach to modeling, compared to the complex methods requiring discretizing the flow regime.

In the present work a more comprehensive set of conditions, such as elevated temperatures indicative of fuel cell operation, were evaluated for the mathematical model used in HVAC energy recovery ventilator (ERV) systems. Some of the simplifications and assumptions made during the mathematical derivation by Zhang and Niu are analyzed for the situation in PEMFC membrane heat and humidity exchangers. The results of an alternative approach were compared with results using the method proposed by Zhang and Niu. Moreover, experiments were conducted with two different types of

membrane, and correlations were found demonstrating that the proposed model can accommodate the data and predict water transfer in membrane humidifiers.

**Table 1.4:** Summary table comparing relevant past research from Zhang and Niu [29,31,32], Huizing [25], Cave [26], Chen and Peng [19,22], Monroe and Romero [24], Park, Choe, Choi [21], and Park and Oh [20,33]

| | Fuel cell conditions | Multiple membranes | General architecture | Overall approach | Model | Experimental | Comments |
|---|---|---|---|---|---|---|---|
| Zhang and Niu (1999-2002) | | × | × | × | × | × | Expanded the effectiveness-NTU method of heat exchangers for latent transfer; atmospheric conditions only; experiments conducted with cross flow energy recovery ventilators |
| Huizing (2007) | × | × | | × | | × | Reported on a simple empirical method to aid in design of planar PEMFC membrane humidifiers; reported on a variety of membranes for possible use in PEMFC humidifiers |
| Cave (2007) | × | | | | × | × | Developed a discretized thermodynamic model based on Nafion planar PEMFC humdifiers; applied part of the latent effectiveness method to discretized model |
| Chen and Peng (2005, 2008) | × | | × | | × | × | Developed a dynamic and static thermodynamic model for a Nafion tube-and-shell PEMFC humidifier; validated model using a Perma Pure humidifier with fitted diffusion coefficient |
| Monroe and Romero (2008) | × | | | | × | × | A complex analytical model was developed for planar Nafion membranes for determining interfacial kinetics, and was correlated with experimental data from simple chamber tests |
| Park, Choe, Choi (2008) | × | | | | × | × | A dynamic and static thermodynamic model was created based on a Nafion shell-and-tube humidifier, and validated for different flow rates only; different geometric factors were experimentally studied using Perma Pure humidifiers |
| Park and Oh (2005, 2008) | × | | | × | × | × | Provided a 1D analytical model using permeability, applied to planar Nafion PEMFC humidifiers; liquid-to-gas only, with some redundant results |
| Kadylak (2009) | × | × | × | × | × | × | Extension of latent effectiveness to PEMFC gas-to-gas membrane humidifiers, with a divergence from Nafion and analysis of 2 different types of membrane; the thermodynamic model is validated with experiments |

In summary, the contributions to the knowledge field presented in this thesis are:

- Evaluation of performance metrics, identifying the most appropriate for fuel cell membrane humidifiers;

- Characterization of the sorption isotherms, water transfer performance, and diffusivity of two different types of membranes;
- A simple humidifier model, yet comprehensive enough for use with PEM fuel cell applications; and,
- Validation of the heat and mass transfer model with experimental data.

## 1.6. THESIS OVERVIEW

Figure 1.4 lays out the overview of this thesis. The introduction is presented first which ends in the previous section with a literature review of recent relevant investigations pertaining to membrane humidification. The next chapter outlines the experimental setup as a precursor to all the experiments that follow in the research presented. A study evaluating the different performance measures and a study on the parameters affecting water transfer are given within that chapter. Another subsection in Chapter 2 is about membrane characterization, which is required before getting into the heat and mass transfer model. The second chapter ends with the results of the independent experiments conducted on the two different membranes. With the background provided, Chapter 3 goes into the simple thermodynamic model based on heat exchanger design methodology, which is at the core of the thesis. The validation of the model with the experimental data obtained and presented in Chapter 2 concludes the chapter on the thermodynamic model. Finally, conclusions and thoughts on further work are presented in the last chapter.

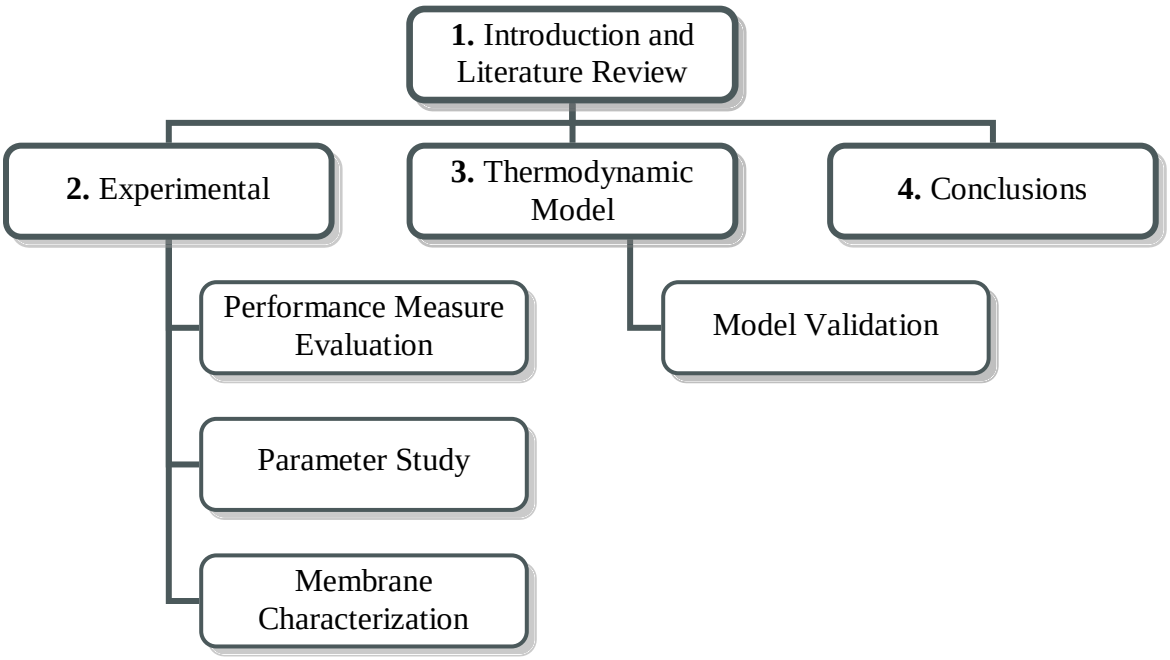


**Figure 1.4:** Overview structure of thesis

# 2. EXPERIMENTS

## 2.1. EXPERIMENTAL SETUP

### 2.1.1. TEST STATION

An Arbin 50 W Fuel Cell Test Station (FCTS) which was used to conduct the model validation and membrane experiments is schematically shown in Figure 2.1. Dry compressed air from the laboratory is supplied to the back of the test station. A tee in the tubing was introduced to supply what would later become the wet and dry streams. For the dry stream, the air passes through a mass flow controller to regulate the flow rate. The dry air is then heated to the desired temperature, before entering the dry inlet port of the humidifier, which has been submerged in an isothermal water bath kept at a constant temperature, $T_{iso}$. For the wet stream, the compressed air first passes through a mass flow meter, then through a water gas bubbler, set at $T_{dp,wi}$, where the stream's temperature will also be raised close to $T_{dp} = T_{dp,wi}$. It will then be heated to the preset $T_{wi}$ temperature, which is generally set at a higher temperature than the dew point temperature $T_{dp,wi}$ to prevent condensation, before entering the wet inlet port of the humidifier. Both streams are exhausted to atmosphere to prevent any backpressure, as indicated in Section 0. At the dry outlet the humidity sensor is placed in line with the stream to capture the wet outlet temperature and humidity. The humidity sensor used is the HMT337 series of the Vaisala Humidicap humidity and temperature transmitter. The sensor has a relative humidity accuracy of 1.5% + 1.5% of the reading over a range of –40°C to 180°C. This translates into a dew point temperature accuracy of 1°C or better in the range of test temperatures and at a relative humidity of at least 56% [34]. This polymer-based

capacitive humidity sensor is also placed in contact with the water in the water bath to maintain the same temperature.

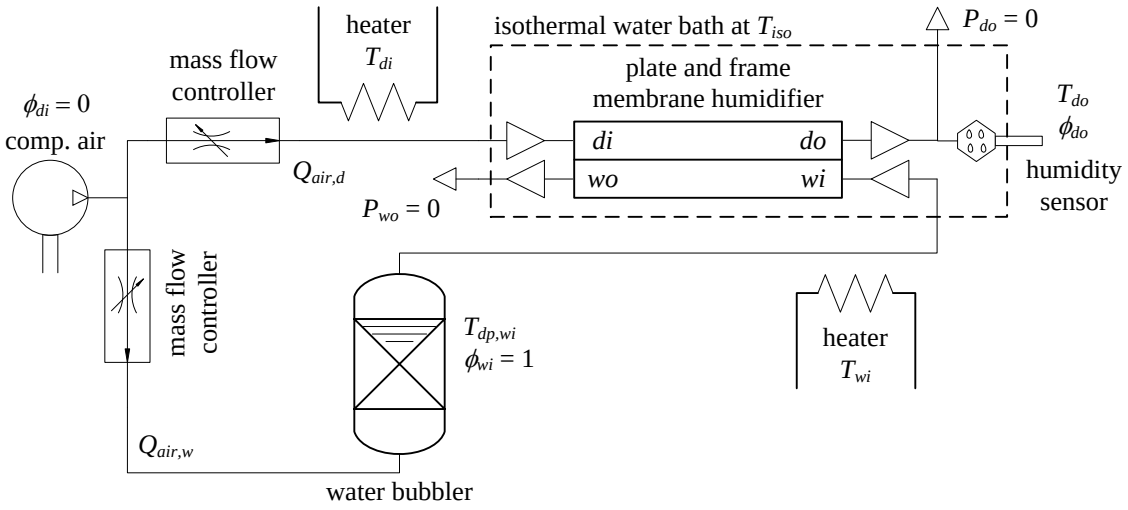


**Figure 2.1:** Experimental setup of test station in line with test humidifier

Preliminary testing on the effects of pressure and temperature parameters, along with the performance metric evaluations, was performed on a Greenlight Power 5 kW G6820 test station with a plate-and-frame membrane prototype humidifier. The test setup follows much the same as outlined in Figure 2.1 without the isothermal water bath. An exception is the use of a contact spray humidifier instead of the gas bubbler to attain the desired dew point temperature of the wet stream. Another difference was the use of gravimetric water balance measurements instead of using a humidity sensor to obtain the amount of water transferred over a period of time, typically 10 min.

### 2.1.2. HUMIDIFIER

The humidifier used in the membrane and validation experiments was a single layer plate-and-frame single cell as shown in Figure 2.2. It is made from two plates of 1 in thick acrylic, with seven channels in parallel machined 1 mm deep. The channels are 3

mm wide and are separated by 1.5 mm lands. The flow enters and exits each side through push-connect elbow adaptors and then spreads out to the seven channels. The membrane sample to be tested is placed in between each plate, with a 0.05 mm PTFE film creating a seal on either side of the membrane and acrylic plate. The entrance and exit areas of the membrane are covered with a thin sheet of water and air-impermeable polyimide film so that only the channel areas are exposed to the flow, eliminating any entrance and exit effects on water transfer and allowing the flow to become fully developed. The channel length exposed for water transport is 135 mm. Four ports have been made available to allow thermocouples to be placed into the flow and measure the temperature of each stream. A Type T thermocouple was placed through a hole drilled in a plastic pipe fitting plug.

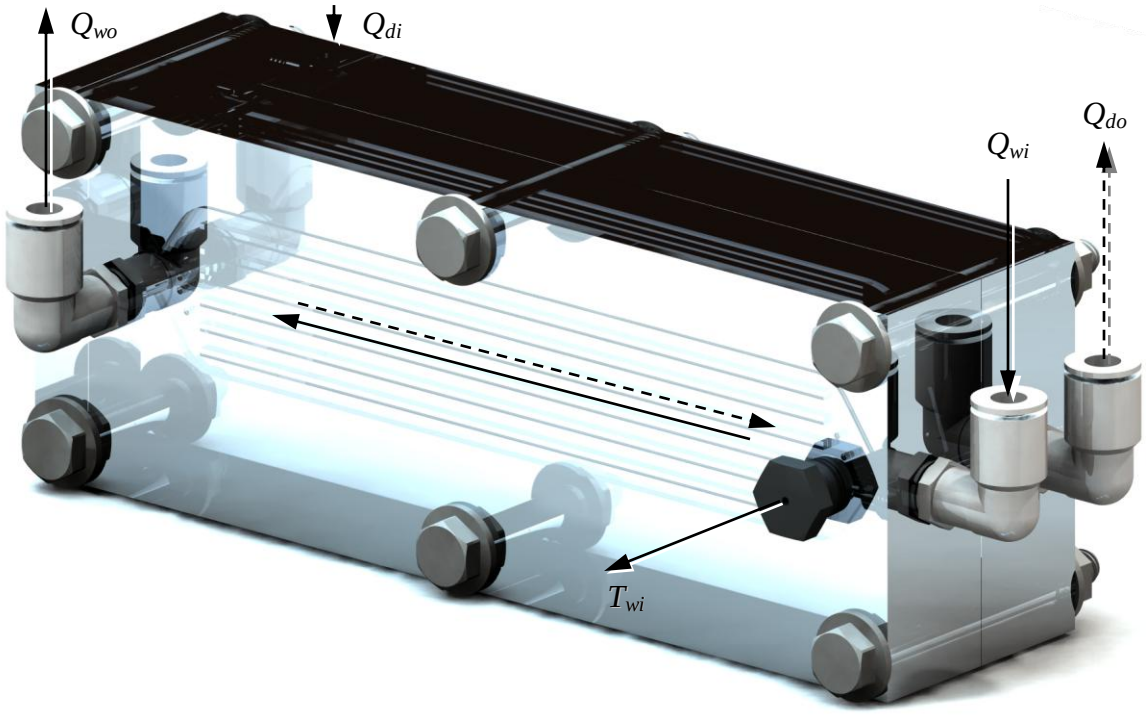


**Figure 2.2:** Experimental single cell humidifier with installed ports

A full subscale prototype humidifier was used for the initial performance metric and parameter study tests. The humidifier was a dPoint Technologies Px3-46mm consisting of 40 plates of 16 channels each, with a perfluorinated composite ionic membrane. The housing of the humidifier was made from polyester to provide rigid support and keep the humidifier insulated.

### 2.1.3. MAINTAINING ISOTHERMAL CONDITIONS

Isothermal conditions were necessary to prevent any condensation from occurring within the test module, as this would introduce another factor which is a challenge to model. Constant-temperature conditions allow for a controlled environment in which the water transfer can be isolated from any heat transfer that may occur in a humidifier, and focuses the study on the water transport across the membrane being tested. To this end, the humidifier was submerged in water contained in a Cole-Parmer BT-15 heated circulating water bath, along with the hollow adaptor which housed the humidity sensor. The connections were made as close as possible to the water level, hence the upright orientation as shown in Figure 2.2. The water bath was kept at 1°C higher than the wet side dew point to prevent condensation when the test station feedback control overshot the dew point temperature set point. The inlet gas temperatures were also set higher than the dew point so as to prevent condensation, and the thermocouples placed in the humidifier at the inlet or outlet of each stream provided feedback for the test station gas temperature set point.

## 2.2. EVALUATION OF PERFORMANCE MEASURES

Experiments were conducted to determine how the humidifier performance varied with changes in operating temperature or in pressure differential across the membrane.

The first experiment was to run the humidifier with the wet and dry inlet streams set with equal temperatures, ranging from 65°C to 80°C, at 100 SLPM and no backpressures. The performance of the humidifier is plotted in terms of the dew point approach temperature, water transfer rate, and water recovery ratio in Figure 2.3. The DPAT compensates for using dew point temperature alone in that the performance decreases in terms of DPAT as temperature increases, yet the actual dry outlet dew point temperature increases. Only using the dry outlet dew point temperature would be misleading, as an increase in dew point does not necessarily mean better performance. On the other hand, the water transfer rate is increasing as the temperature increases, but this can be explained by the fact that there is more water mass available to be transferred for the higher saturated wet inlet temperatures. The water recovery ratio accounts for the extra water that is available as the temperature increases, and shows that the humidifier performance decreases in relative terms as the inlet temperatures increase.

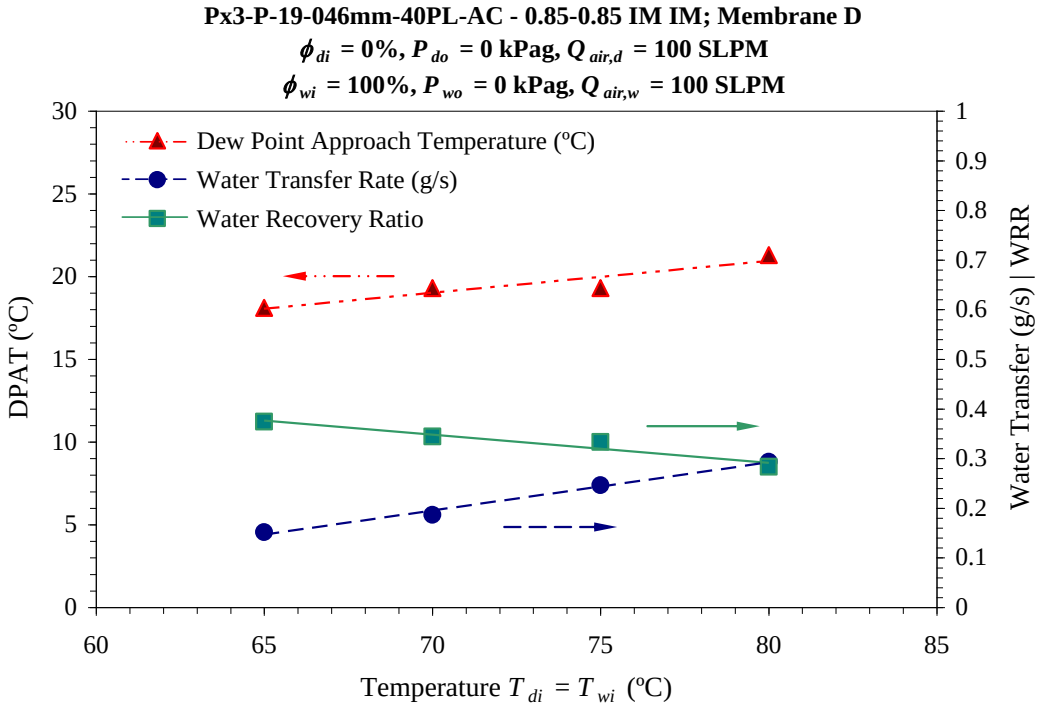


**Figure 2.3:** Water transfer as operating temperature is changed

In the second experiment, the dry inlet stream was kept at 25°C and the wet inlet stream was supplied saturated at 65°C, both streams with an air flow rate of 100 SLPM. This time the dry outlet backpressure was increased from ambient to 35 kPag, while keeping the wet outlet backpressure at atmospheric pressure, creating a pressure differential across the membrane of up to 35 kPa. This is equivalent to a pressure ratio of up to 1.35 (136 kPaa/101 kPaa). The dew point approach temperature, water transfer rate, and water recovery ratio are once again plotted, this time in Figure 2.4. In the previous experiment, the slopes of the DPAT and WRR diverged, while in this experiment the slopes are both negative. In this case, the DPAT signifies that the humidifier is performing better as the pressure differential increases, yet both the water transfer rate and WRR suggest that the humidifier is actually performing worse as the pressure differential increases. In conclusion, the dew point temperature or dew point approach temperature is a misleading measure of humidifier performance, and should be avoided. In both experiments, the same amount of membrane area was used, so the water flux would give the same results as the water transfer rate. The absolute measure of water transfer rate does not adequately account for the change in available water at different flow conditions for the same humidifier; though it may be a good measure for comparing different humidifiers at the same operating conditions. A better measure is the water recovery ratio, which takes into account the amount of water supplied as the operating conditions change; however, it is difficult to determine if an adequate amount of water is supplied to the fuel cell with the water recovery ratio alone, so the necessary WRR would need to be calculated beforehand based on the operating conditions. Therefore, because the required operating conditions of the fuel cell will change with loading, it is proposed

that water recovery ratio be used as the preferred performance metric, as it will take into account the different amount of water supplied at each flow rate and flow conditions.

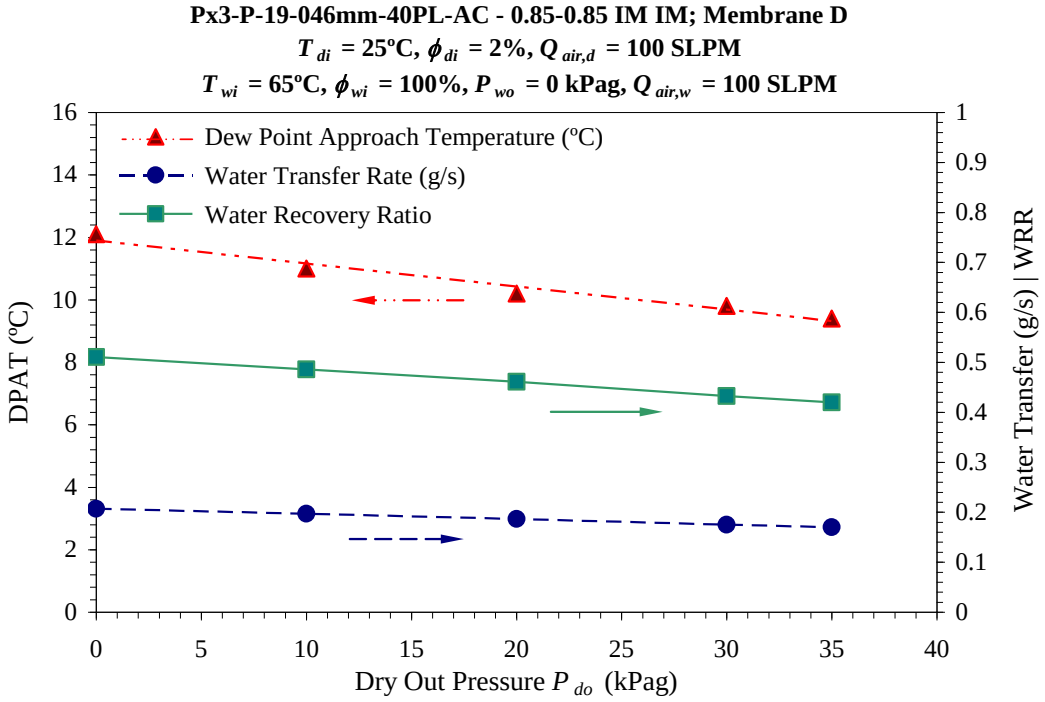


**Figure 2.4:** Water transfer as dry stream pressure is changed

## 2.3. PARAMETER EFFECT STUDY

As can be seen from Section 1.4, there are many variables that could be studied, resulting in a very large experimental matrix. To determine if the potential experimental matrix could be condensed by eliminating a possible variable, such as temperature or pressure, the plate-and-frame membrane prototype humidifier described in Section 2.2 was tested on the same Greenlight Power 5 kW G6820 test station.

The first test conducted was to increase the dry incoming air temperature in increments of 5°C until it met the wet inlet temperature, maintained at 80°C, with ambient backpressures on both streams. The range of temperature was chosen such that it represented the typical range found in operating fuel cell temperatures, with the minimum

temperature taken to be close to room temperature, or 25°C. These dry inlet temperatures were normalized over the range of operating conditions to facilitate comparison with pressures in the subsequent experiments. The testing conditions are outlined in Table 2.1, and the results of the temperature dependence test are displayed in Figure 2.5. Linear regression analysis of the dry outlet dew point against normalized temperature data demonstrates a slope of –8.17°C ($R^2$ = 0.935).

**Table 2.1:** Experimental matrix for temperature-dependence testing

| Membrane | Control | Flow Rate | Temperature ($T_{di}$) | | | Dependent |
|---|---|---|---|---|---|---|
| Membrane D: perfluorinated ionic composite | $T_{wi} = T_{dp,wi}$ = 80°C<br>$T_{dp,di}$ = –20°C<br>$P_{do} = P_{wo}$ = 0 (gauge) | 100 SLPM | 25°C | … | 80°C | WRR<br>$T_{do}$<br>$T_{dp,do}$ |

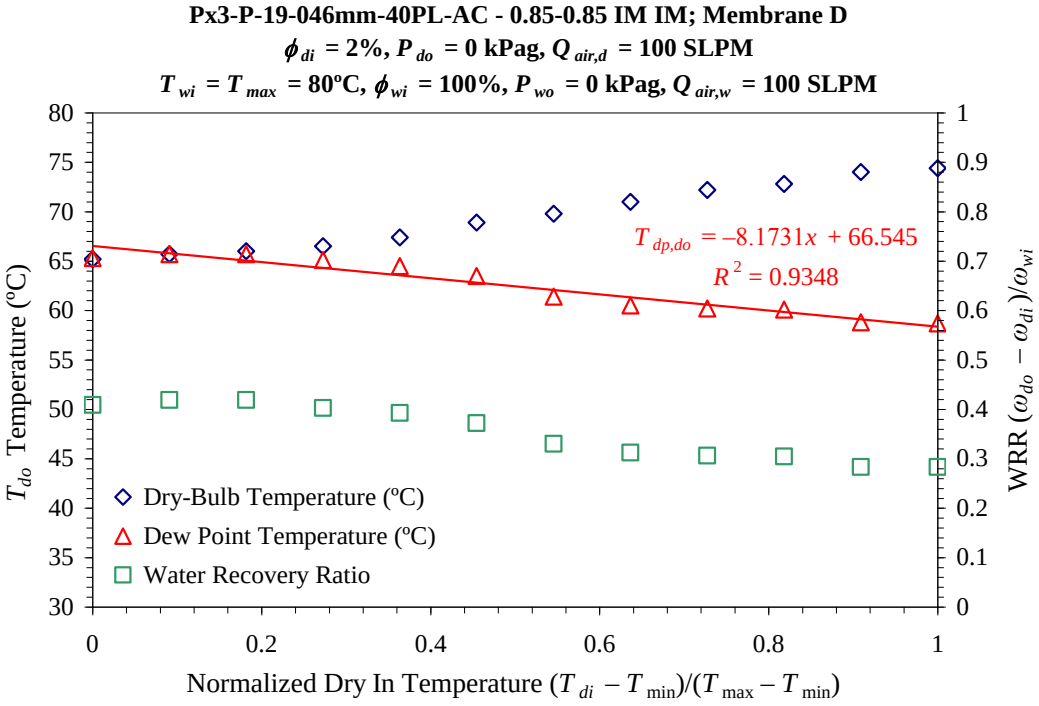


**Figure 2.5:** Effect on water transfer of changing dry inlet temperature

The next test performed was to maintain constant inlet temperature while changing the dry air outlet backpressure from ambient to 35 kPa gauge. The range of

pressure observed across the membrane is dictated by the pressure drop across a fuel cell stack, which is normally below 5 psi (35 kPa). These dry outlet pressures were normalized and the results of this test are shown in Figure 2.6. Linear regression ($R^2$ = 0.97) through the dry outlet dew point temperature points in this graph gives a slope of 2.58°C. Table 2.2 outlines the testing conditions of both pressure dependence tests.

**Table 2.2:** Experimental matrix for pressure-dependence testing

| Membrane | Control | Pressure (kPag) $P_{wo}$ | $P_{do,\min}$ | $P_{do,\max}$ | Dependent |
|---|---|---|---|---|---|
| Membrane D: perfluorinated ionic composite | $T_{wi} = T_{dp,wi} = 65°C$<br>$T_{di} = 25°C$; $T_{dp,di} = -20°C$<br>$Q_{air,d} = Q_{air,w} = 100$ SLPM | 0 | 0 | 35 | WRR<br>$T_{do}$<br>$T_{dp,do}$ |
| Membrane D: perfluorinated ionic composite | $T_{wi} = T_{dp,wi} = 65°C$<br>$T_{di} = 25°C$; $T_{dp,di} = -20°C$<br>$Q_{air,d} = Q_{air,w} = 100$ SLPM | 120 | 120 | 155 | WRR<br>$T_{do}$<br>$T_{dp,do}$ |

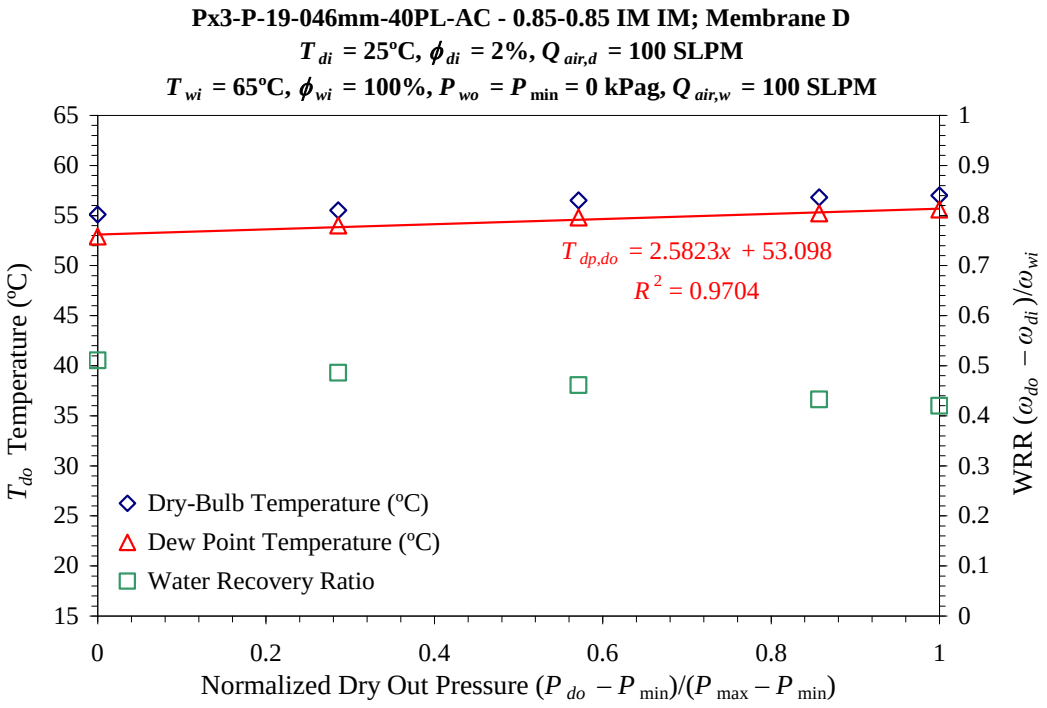


**Figure 2.6:** Effect on water transfer of changing dry out backpressure, low total pressure

Operation at elevated pressures is required for many fuel cell systems, such as in automotive applications, so a similar test was performed at these pressures. Even at elevated pressures, the fuel cell stack will rarely incur pressure drops greater than 5 psi (35 kPa). In this test the dry outlet backpressure ranged from 120 kPag to 155 kPag, while maintaining the wet outlet backpressure at 120 kPag. The outcome is displayed in Figure 2.7. The dry side outlet pressures were likewise normalized in the plot.

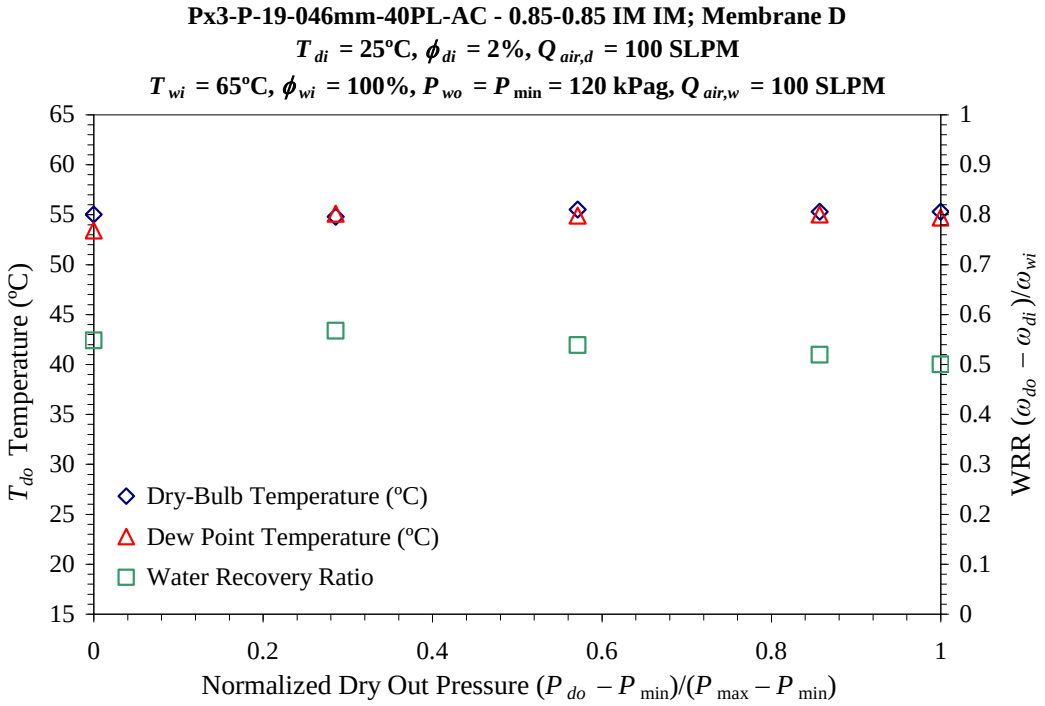


**Figure 2.7:** Effect on water transfer of changing dry out backpressure, high total pressure

At the high total pressures, the effect of changing the pressure in one gas stream has little effect on the water transfer. Likewise, at the lower total pressures—close to atmospheric pressure—comparing the slopes of the best fit lines reveals that the temperature difference between the inlets of the streams plays a larger role on water transfer than pressure difference between streams for the range of temperature differences

and pressure differences seen in practical fuel cell operation. Therefore, since the dry side outlet dew point temperature varies by up to a factor of three over the tested range, it was decided that the effect of temperature would be the focus of the ongoing analysis of membrane water transfer in plate-and-frame humidifiers, and that the effect of pressure would be neglected by conducting all simulations and experiments at atmospheric conditions.

## 2.4. MEMBRANE CHARACTERIZATION

### 2.4.1. SOLUTION-DIFFUSION AND SORPTION CURVES

In porous solid membranes, the main mechanisms of water transfer are surface diffusion into the membrane and liquid flowing through the membrane by capillary condensation. A water concentration gradient from the water molecules adsorbed on the pore walls and diffusing on the surface is the driving force in surface diffusion [35]. The primary mass transfer of permeating species from the wet side to the dry side can be broken down into three steps [32]; i.e.:

1. Adsorption at the supply side of the membrane;
2. Diffusion through the membrane as described by adsorption isotherms;
3. Desorption at the sweep side of the membrane.

Solution-diffusion theory models water transport as a flux proportional to a driving gradient. Analogous to the conduction equation in heat transfer known as Fourier's Law, in the case of mass diffusion the diffusion equation for flux of species A in medium B is known as Fick's Law, and the proportionality constant is the binary diffusion coefficient or mass diffusivity, denoted by $D_{AB}$ [28]:

$$J_A = -D_{AB} \nabla \Phi_A \tag{11}$$

where $\Phi$ is a placeholder variable for the potential driving force, which may be mass based (density), mol based (concentration), chemical potential based, etc. Depending on the driving force chosen, the diffusivity will need to be adjusted or multiplied by a factor to maintain the correct units.

For a membrane with a hygroscopic polymer component, water transport increases with an increase in humidity. For these types of membranes, a sorption isotherm (or water uptake curve) provides the response of the membrane with change in average relative humidity. On the other hand, if the pore structure is large enough, such as in porous textiles, water vapor will transport through the gas-filled pore structure. In these membrane types, generally not suitable for PEMFC humidification due to air cross-over, water vapor diffusion does not depend on relative humidity since the water vapor simply diffuses through pore voids [36].

For membranes which exhibit small diffusion coefficients requiring long experiment times, the sorption technique is preferred to the permeation technique [37]. The sorption technique of quantifying water uptake is performed using a dynamic gravimetric vapor sorption (DVS) instrument. A small sample of the membrane (< 1 $cm^2$) is suspended on a quartz spring, which measures the weight of the membrane as it absorbs or desorbs water with an ultra-microbalance. The membrane is kept in a chamber where the temperature and humidity are controlled by mixing saturated and dry carrier gas streams through mass flow controllers, and the whole instrument is kept in an incubator to keep it isothermal [38]. The sorption isotherms of two different membranes, which will be later used in the study, are described in the next two sections.

### 2.4.2. WATER UPTAKE OF A HYDROPHILIC-IMPREGNATED POLYMER

Much testing and data have been collected on DuPont Nafion$^{TM}$ membranes in industry and in the literature. However, due to their exorbitant cost they are not expected to be used in future humidifier systems, hence the need to acquire more commercially feasible membranes as outlined in the Introduction. Furthermore, there are disparate data on Nafion's sorption and diffusivity values in the literature, as reported by Cave [26], making it difficult to use for practical modeling. With this in mind, it was decided to concentrate on a commercially available membrane. The chosen porous-type membrane is made from a hydrophilic-filled polymer. It has a porosity of approximately 70%, thickness of 0.15 mm, and hydrophilic additive to polymer ratio of 2.5. It further contains 15% plasticizer mineral oil used in the extrusion process. Due to its commercial availability, this membrane (labeled Membrane E), is very low in cost, in the range of \$3/m$^2$. The membrane is coated in a 4% Nafion (PFSA) DE2021 dispersion to decrease the air crossover, and baked at 100°C for 1 h to help anneal the Nafion.

Three samples of the porous polymer with hydrophilic additive membrane were characterized using a Surface Measurement Systems (UK) vapor sorption instrument as described in the previous section. The samples' sorption and desorption curves were characterized at 25°C, as past attempts to perform experiments at high temperatures on the DVS equipment have failed. Each sample was first dried to < 1% relative humidity to determine its dry mass. The relative humidity was then increased stepwise in 10% increments up to 90%, then to 94% and 97%. The relative humidity was then decreased following the same profile to obtain the desorption curve. Mass equilibrium was obtained at each step before moving on to the next humidity setting. Mass equilibrium was reached when the change in mass with respect to total mass of the sample was less than 0.1%, or

$dm/dt$ < 0.001. The sorption and desorption profiles were discovered to be nearly equal. All six profiles (three absorption and three desorption) of the porous polymer-hydrophilic additive membrane with PFSA coating were averaged and are plotted with their 95% confidence interval error bars in Figure 2.8. A third-degree polynomial was used to curve fit the data up to 80% relative humidity, with an $R^2$ value of 0.996. The curve past 80% relative humidity is then fitted to a general isotherm curve for water uptake $\theta$:

$$\theta = \frac{\theta_{\max}}{1 - C + C/\phi} \tag{12}$$

where the maximum moisture content is $\theta_{\max}$ = 2.5, and the value of constant $C$ = 148. With a value of C in the order of 100, indicating a low uptake for most of the low end of relative humidity and a sharp slope at the very high end of relative humidity, this porous membrane is characterized as Type III Extreme (Type IIIE) [39]. Several desiccant polymers exhibit Type III behavior, with a great increase in uptake only at values greater than 90% relative humidity [32].

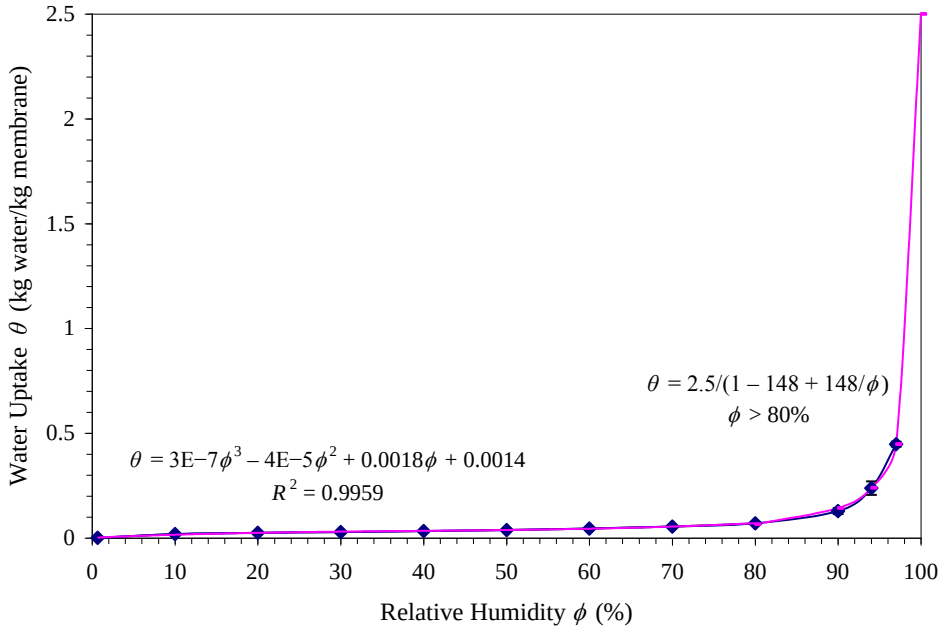


**Figure 2.8:** Sorption isotherm at 25°C of hydrophilic additive-impregnated porous polymer membrane

Due to limitations encountered in the past with using the dynamic vapor sorption instrument, an isotherm was only obtained at 25°C; however, up to moderate temperatures the sorption curve tends to be independent of temperature [40].

### 2.4.3. WATER UPTAKE OF A PERFLUORINATED COMPOSITE MEMBRANE

One of the disadvantages of the porous polymer membrane is its limited lifetime in fuel cell operation. It has been hypothesized that the physical adhesion between hydrophilic additive and polymer degrades under wear, leading to the loss of hygroscopic additive from the polymer matrix [25]. A new membrane has been obtained which has logged over 5000 h at fuel cell operating conditions without degradation compared to the approximately 3000 h lifetime experienced by the incumbent, baseline porous polymer membrane described in the previous section. The new membrane is an ionic composite, with a middle layer of perfluorinated composition, and hydrophobic outer layers. As described earlier, an ionic membrane has a water transport mechanism similar to that of Nafion, where clusters of water are transported across the thickness of the membrane due to the ionic bases. The overall thickness of this membrane is 0.02 mm. This membrane is proprietary technology, so its description must be kept confidential.

The vapor sorption experiment was repeated with samples of the ionic perfluorinated composite membrane. The experimental temperature (25°C) and relative humidity profile was kept the same as with the polymer-hydrophilic additive membrane. The sorption isotherm is displayed in Figure 2.9. With a maximum water uptake of $\theta_{max}$ = 0.217, and the value of $C$ = 9.23, this membrane also exhibits Type III behavior, only experiencing increased water uptake at high relative humidities. A third-degree

polynomial fit ($R^2$ = 0.999) was also obtained for relative humidities less than 80% to be integrated into the model.

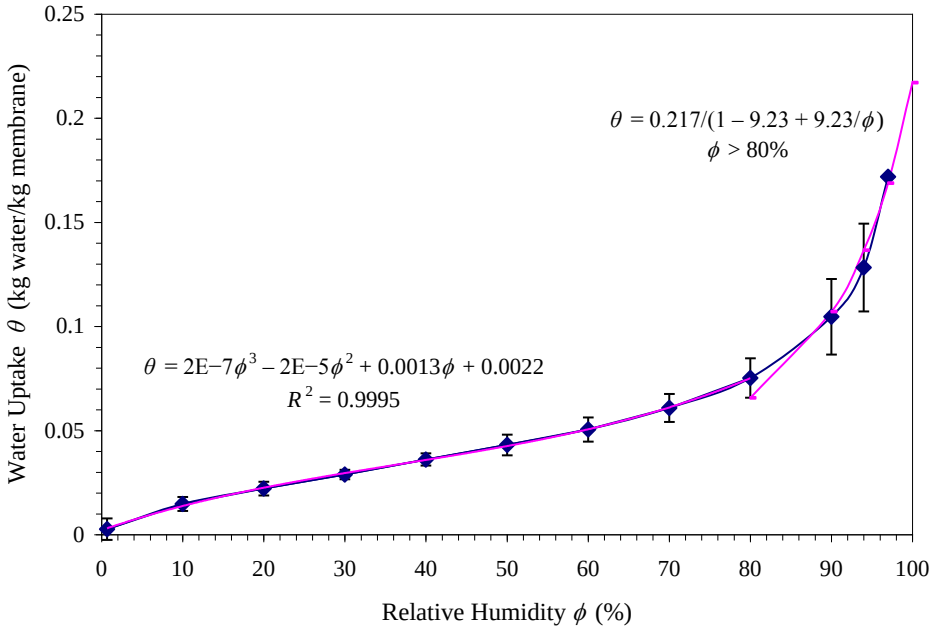


**Figure 2.9:** Sorption isotherm at 25°C of ionic perfluorinated composite membrane

### 2.4.4. COMPARISON OF THE POROUS AND IONIC MEMBRANES

The sorption isotherms of the polymer-hydrophilic additive, PFSA coated and perfluorinated composite membranes were plotted on the same graph in Figure 2.10. The two membranes show the same water uptake characteristics up to 80% relative humidity. However, the porous polymer membrane exhibits a much higher maximum water uptake compared to the ionic perfluorinated composite membrane. At 97% relative humidity, the porous membrane is able to absorb 2.6 times as much water as the ionic membrane on a membrane mass basis, which already takes into account the thickness of each membrane. One hypothesis, in accordance with observation, is that the porous polymer membrane, being hydrophilic, absorbs liquid water into the structure of the membrane. Whereas the ionic membrane, with its hydrophobic outer layers, prevents liquid water from wetting on

the surface and therefore inhibits water absorption, or due to the fact that a high weight percentage of the membrane is the hydrophobic layers, which does not sorb water vapor.

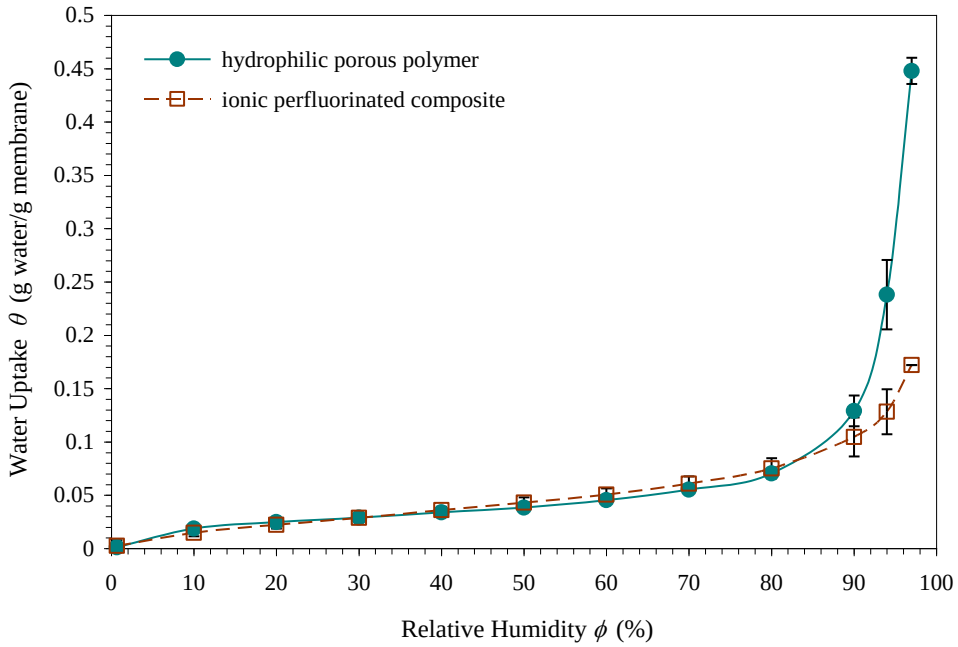


**Figure 2.10:** Comparison of sorption isotherm at 25°C of a porous and an ionic membrane

## 2.5. EXPERIMENTAL DESIGN

The mathematical model developed in Chapter 3 requires some fitted parameters, such as the diffusivity of water in the membrane, in order to be adequately used over a range of temperatures. This chapter lays out the experiments undertaken to validate the model, to gain confidence in its results and to obtain the values for parameters described in Section 3.7 that are required for its practical use. Once the model has been verified, it will then be ready to be used for different conditions or different geometries, more in accord with the scale of commercial products. The dependent variable to be obtained will be the water transfer as taken from measurements of water at the outlet of the dry stream.

### 2.5.1. TEST MATRIX AND CONDITIONS

A difference in fuel cell humidification as compared to ERV systems is that the wet stream entering the humidifier is generally saturated. Heat transfer occurs when there is a difference in temperature. Thus, water condensation, and hence two-phase flow, is inevitable in the wet flow of fuel cell membrane humidifiers if there is any temperature difference between the flows or the surroundings. Therefore isothermal conditions are chosen to perform comparison of humidifier performance at different flow rates, and the effects of condensation and two-phase flow are suggested as topics for further investigation.

Since the sorption curves were obtained at 25°C, one set of experiments were conducted at a benchmark temperature of 25°C, even though fuel cell systems will for the majority of their time operate at higher temperatures. As discussed in Section 3.4.1, an average fuel cell operating temperature of 50°C is more appropriate for backup and portable applications. This gives another temperature at which to conduct experiments. There is also a trend to operate fuel cells at higher temperatures, as in forklift and automotive applications. From a survey of customer specifications available to dPoint Technologies for applications at higher temperatures, another operating temperature was chosen at 75°C. Therefore, the experiments to be conducted are three equally spaced isothermal temperatures: 25°C, 50°C and 75°C.

It is necessary to test a range of flow rates; both because the humidifier will see different demands as the fuel cell operates through a range of power, and because it is required in determining the rated flow of a certain humidifier design. Due to the large number of plates to divide the flow, a plate-and-frame humidifier will always run at laminar flow, even though design elements may be introduced to cause flow separation

and therefore enhance heat and mass transfer. A particular plate-and-frame humidifier designed at dPoint for backup power applications may see a Reynolds number of 80. The proposed test jig for the humidifier experiments has 7 channels with 1 mm height and 3 mm width, with one layer for each stream. The hydraulic diameter, $D_h$, is found from:

$$D_h = \frac{4wd}{2(w+d)} = 1.5 \text{ mm} \tag{13}$$

The Reynolds number is defined as

$$\text{Re} = \frac{\rho D_h Q}{\mu w d} \tag{14}$$

Rearranged to find the flow rate per channel, $Q$, using the 75°C isothermal case to obtain the dynamic viscosity of air $\mu = 2.07 \times 10^{-5}$ kg m$^{-1}$ s$^{-1}$, and its density at STP $\rho$ = 1.29 kg m$^{-3}$:

$$Q = \frac{\text{Re } \mu w d}{\rho D_h} = 0.154 \text{ SLPM} \tag{15}$$

The flow rate per stream is found by multiplying by the number of channels, $n$ = 7, so that the flow rate for each side is 1.08 SLPM. An Arbin 50 W Fuel Cell Test Station (FCTS), which has mass flow controllers rated up to 1.1 SLPM and 2 SLPM for two separate streams, was used to supply metered dry air and saturated wet air. With the limitation of 1.1 SLPM of one stream in mind, the flow rates to be tested are at 0.4, 0.7, and 1 SLPM.

The dry stream of the humidifier will be at a lower flow than the wet stream because the air component coming out of the fuel cell stack will have depleted oxygen content, having reacted with hydrogen to form water; however, the ratio of air flows on the dry side compared to the wet side varies according to the stoichiometry used to

supply the fuel cell with extra oxygen to react with. The higher the air stoichiometry supplied, the closer the air flow rate on the dry side will be to the air flow on the wet side. For this reason, a simplification is applied where the dry side and wet side air flows are maintained equal. Water is added to the wet side air flow from a gas bubbler to saturate the air at the given test temperature, and this water flow rate is not included in the test conditions as wet air does not pass through the mass flow controller. The dry air is supplied from a compressed air line, which has been measured to have a relative humidity between 0.16% and 2.9% through the whole test temperature range (or always lower than a –20°C dew point temperature).

As outlined in Section 0, the focus of the study is on temperature effects over pressure effects on water transport in practical operation, so the outlets are kept at ambient pressure. Since the chosen performance measure to be tested is the water transfer from the wet side to the dry side, water recovery ratio (WRR) is the dependent variable to be sought in the tests. The amount of water at the dry outlet will also be presented by the dew point $T_{dp,do}$ as a measure of the amount of water available to the fuel cell, which is one of the parameters of water outputted by the humidity sensor. All the foregoing variables and testing conditions as inputs and the output are laid out in the test matrix of Table 2.3.

**Table 2.3:** Experimental testing matrix

| Membrane | Control | Flow Rate | Temperature ($T_{iso}$) | | | Dependent |
|---|---|---|---|---|---|---|
| Membrane E: porous polymer, PFSA coated | $T_{di} = T_{wi} = T_{dp,wi} = T_{iso}$<br>$T_{dp,di}$ = –20°C<br>$P_{do} = P_{wo}$ = 0 (gauge) | 0.4 SLPM<br>0.7 SLPM<br>1 SLPM | 25°C<br>25°C<br>25°C | 50°C<br>50°C<br>50°C | 75°C<br>75°C<br>75°C | WRR ($T_{dp,do}$) |
| Membrane D: perfluorinated ionic composite | As above | 0.4 SLPM<br>0.7 SLPM<br>1 SLPM | 25°C<br>25°C<br>25°C | 50°C<br>50°C<br>50°C | 75°C<br>75°C<br>75°C | WRR ($T_{dp,do}$) |

## 2.6. MEMBRANE RESULTS AND DISCUSSION

Three samples of the Nafion-coated polymer membrane with hydrophilic additive were tested at three different flow rates and at three different temperatures according to the conditions presented in the experimental matrix, Table 2.3, for a minimum of 27 tests. The results of the humidifier performance in terms of water transfer through the membrane are presented in Figure 2.11 with the measured dry outlet dew point temperature from the humidity sensor, and the converted water recovery ratio also plotted.

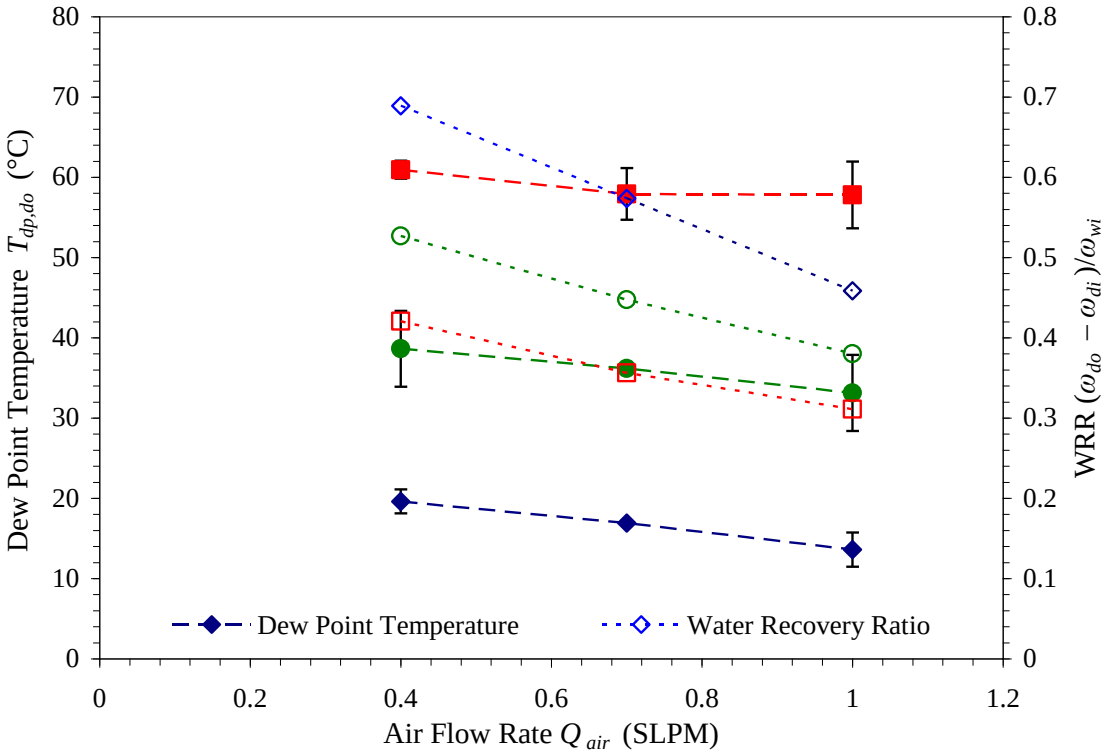


**Figure 2.11:** Experimental results for porous polymer membrane E, at ♦ $T_{iso}$ = 25°C, ● 50°C, ■ 75°C

As expected, the trend at all temperatures shows an inverse relation between flow rate and water transfer: as the flow rate increases, the water transfer relative to amount of supply water will decrease. In terms of water recovery ratio, the effect of decreasing

water transfer with increasing flow rate is more pronounced the lower the temperature, which can be seen with the steeper slopes as temperature decreases. Likewise, humidifier performance suffers at higher temperatures, with water recovery ratios between 31% and 42% at the tested flow rates and geometry for the 75°C isothermal condition, compared to the 46% to 69% WRR at 25°C.

Similarly, three samples of the composite perfluorinated membrane were tested according to the test conditions in Table 2.3, which are the same as for the polymer-hydrophilic additive based membrane. The dry out temperatures and water recovery ratios at the different flow rates are displayed in Figure 2.12.

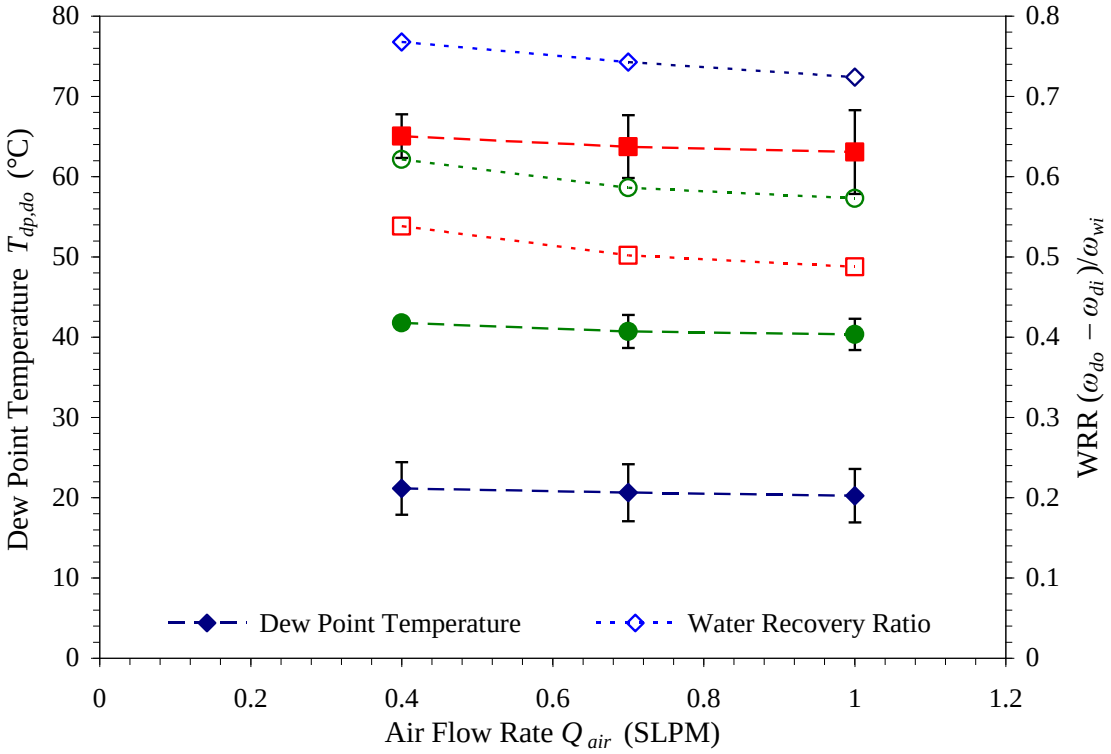


**Figure 2.12:** Experimental results for composite ionic membrane D, at ♦ $T_{iso}$ = 25°C, ● 50°C, ■ 75°C

At the tested conditions the perfluorinated composite membrane showed more constant water transfer rates across the different flow rates tested, as demonstrated by the

nearly flat curves. It is possible this may be attributed to different transfer mechanisms in the membranes. The porous polymer membrane is porous and water absorbs into the membrane enhanced by the hydrophilic Nafion coating, whereas in the ionic composite membrane water is transferred according to the Grotthus mechanism of water-cluster hopping [41,42]; also, the outer layers are hydrophobic preventing wetting and overall absorption into the membrane. Figure 2.13 plots the water recovery ratio of the two membranes. The perfluorinated composite membrane shows greater water transfer at all temperatures and flow rates, from as low as 11% better at 25°C and 0.4 SLPM, and up to 56% better at 1 SLPM. One factor that makes the ionic composite membrane better for water transfer is its thinness—it is approximately 13% as thick as the porous polymer membrane—resulting in decreased diffusivity resistance across the membrane.

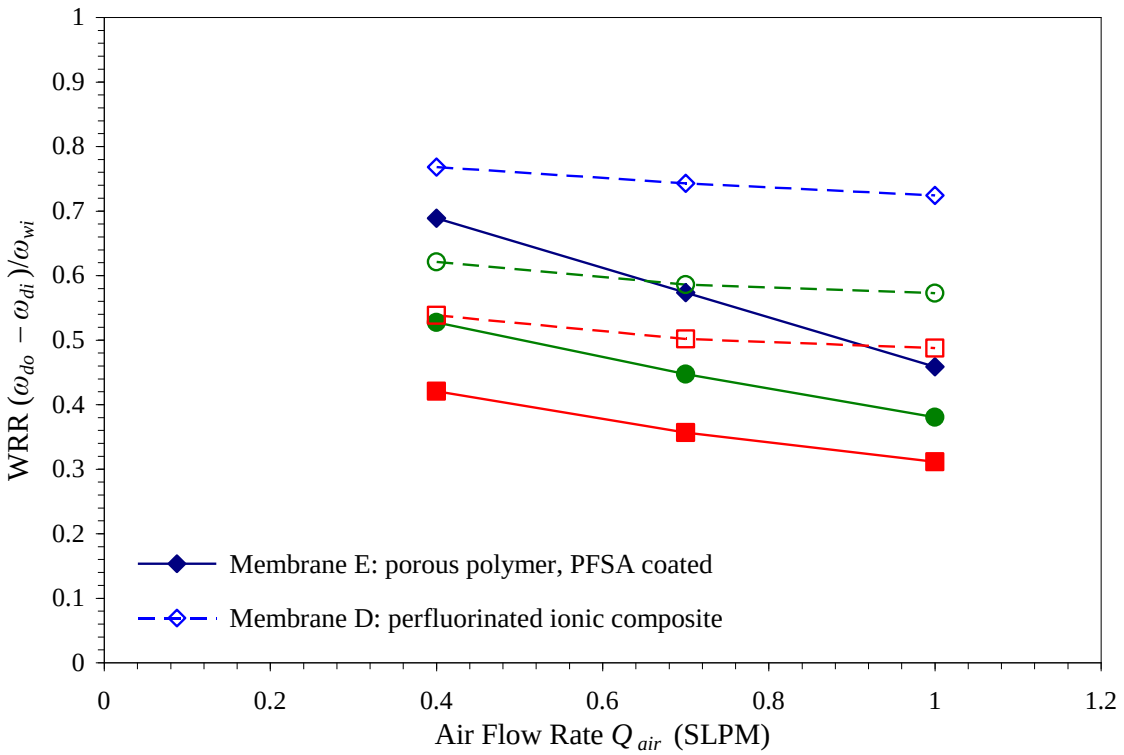


**Figure 2.13:** Comparison of water recovery ratio between two membranes, at ♦ $T_{iso}$ = 25°C, ● 50°C, ■ 75°C

# 3. HEAT AND WATER TRANSFER MODEL

## 3.1. HEAT TRANSFER USING THE EFFECTIVENESS METHOD

In heat exchanger design, given the inlet temperatures (but not the outlet temperatures), the preferred analysis approach is the effectiveness method. This method is used when the flow rates and heat exchanger size and type are known. The effectiveness method can also be used in reverse to size heat exchangers—finding the required number of thermal units (NTU), and then selecting a heat exchanger which meets that NTU based on the outlet flow requirements.

The effectiveness method for heat exchanger design starts by obtaining the number of transfer units, NTU, defined as:

$$\mathrm{NTU} = \frac{UA}{(\dot{m} c_p)_{\min}} \tag{16}$$

where $U$ is the overall heat transfer coefficient and $A$ is the heat transfer area, which are parameters of the heat exchanger design. Common pipe flow heat transfer correlations are used to determine the heat transfer coefficient $h$, and $c_p$ is the specific heat capacity, which is multiplied by the mass flow rate of the fluid $\dot{m}$ . Since the $\varepsilon$-NTU method is an overall approach as opposed to a discretized model, all fluid property must be determined at the average conditions of each stream, based on the inlet and outlet conditions. Likewise, if the temperature of the membrane is required, an average temperature is used, calculated from all stream inlet and outlet temperatures.

The effectiveness, $\varepsilon$, is a ratio of the actual heat transfer rate for a heat exchanger to the maximum possible heat transfer rate in those flow conditions

$$\varepsilon = \frac{q}{q_{\max}} = \frac{(\dot{m}c_p)_w (T_{wi} - T_{wo})}{(\dot{m}c_p)_{\min} (T_{wi} - T_{di})} = \frac{(\dot{m}c_p)_d (T_{do} - T_{di})}{(\dot{m}c_p)_{\min} (T_{wi} - T_{di})} \tag{17}$$

where the dry stream has been taken to be the cold stream, and the wet stream the hot stream. The nomenclature will be dealt with in terms of a drier and wetter stream in order to later apply the equations to a humidifier with hot and cold streams. Rearranging Eqn. (17) one can find the sought-after outlet temperature if the effectiveness is known:

$$T_{do} = T_{di} - \varepsilon \frac{(\dot{m}c_p)_d}{(\dot{m}c_p)_{\min}} (T_{di} - T_{do}) \tag{18}$$

Kays and London have shown that depending on the heat exchanger type, the effectiveness is a function of NTU and $C_r = C_{\min}/C_{\max} = (\dot{m}\ c_p)_{\min}/(\dot{m}\ c_p)_{\max}$ [27].

$$\begin{aligned} \varepsilon &= \frac{1 - \exp[-\mathrm{NTU}\ (1 + C_r)]}{1 - C_r \exp[-\mathrm{NTU}\ (1 - C_r)]}, \quad && C_r < 1 \\ \varepsilon &= \frac{\mathrm{NTU}}{1 + \mathrm{NTU}}, && C_r = 1 \end{aligned} \tag{19}$$

which is the effectiveness for a typical counter flow heat exchanger.

Therefore, knowing the effectiveness and the inlet temperatures in addition to the heat exchanger geometry and configuration enables the determination of the heat transfer rate and hence the outlet temperatures.

## 3.2. THE CHILTON-COLBURN ANALOGY FOR MASS TRANSFER

Zhang and Niu report in [29] and [32] their application of the Chilton-Colburn analogy. The analogy is between heat transfer and mass transfer—derived from the *j* factors for heat and mass transfer—which is stated as:

$$j_H = j_M \tag{20}$$

In Ref. [32], the correct fundamental equations to the Chilton-Colburn analogy are given, such as the *j* factor for heat transfer from the Stanton and Prandtl numbers

$$j_H = \mathrm{St}_H \, \mathrm{Pr}^{2/3} \tag{21}$$

where the Stanton number for heat transfer, using the Nusselt and Reynolds numbers, is

$$\mathrm{St}_H = \frac{\mathrm{Nu}}{\mathrm{Re}\ \mathrm{Pr}} \tag{22}$$

Likewise the *j* factor for mass transfer using the corresponding Stanton number and Schmidt number

$$j_M = \mathrm{St}_M \mathrm{Sc}^{2/3} \tag{23}$$

where the Stanton number for mass transfer, utilizing the Sherwood number, is

$$\mathrm{St}_M = \frac{\mathrm{Sh}}{\mathrm{Re}\ \mathrm{Sc}} \tag{24}$$

Defining the Lewis number as the ratio of thermal diffusivity to mass diffusivity [28,43]:

$$\mathrm{Le} = \frac{\alpha}{D_{AB}} = \frac{\mathrm{Sc}}{\mathrm{Pr}} \tag{25}$$

and substituting Eqn. (21) to (24) into the Chilton-Colburn analogy, Eqn. (20), gives:

$$\left(\frac{\mathrm{Nu}}{\mathrm{Re}\ \mathrm{Pr}}\right)\mathrm{Pr}^{2/3} = \left(\frac{\mathrm{Sh}}{\mathrm{Re}\ \mathrm{Sc}}\right)\mathrm{Sc}^{2/3} \tag{26}$$

Rearranging leads to:

$$\mathrm{Sh} = \mathrm{Nu}\left(\frac{\mathrm{Sc}}{\mathrm{Pr}}\right)^{1/3} = \mathrm{Nu} \cdot \mathrm{Le}^{1/3} \tag{27}$$

which can then be used to find the convective mass transfer coefficient as:

$$h_M = \frac{h}{c_p}\mathrm{Le}^{1/3} \tag{28}$$

Since the values for the Lewis number are usually around unity for typical ERV conditions, if the Lewis number term is ignored in the heat and mass transfer analogy the error is not likely to carry through to a great extent through to the rest of the other parameters, such as the overall mass transfer coefficient $U_L$ used in Eqn. (16). The inclusion of water vapor with air will however have a greater effect on the mass transfer coefficient than of dry air alone, due to deviations from unity in the Lewis number, especially at higher temperatures as shown in Figure 3.1.

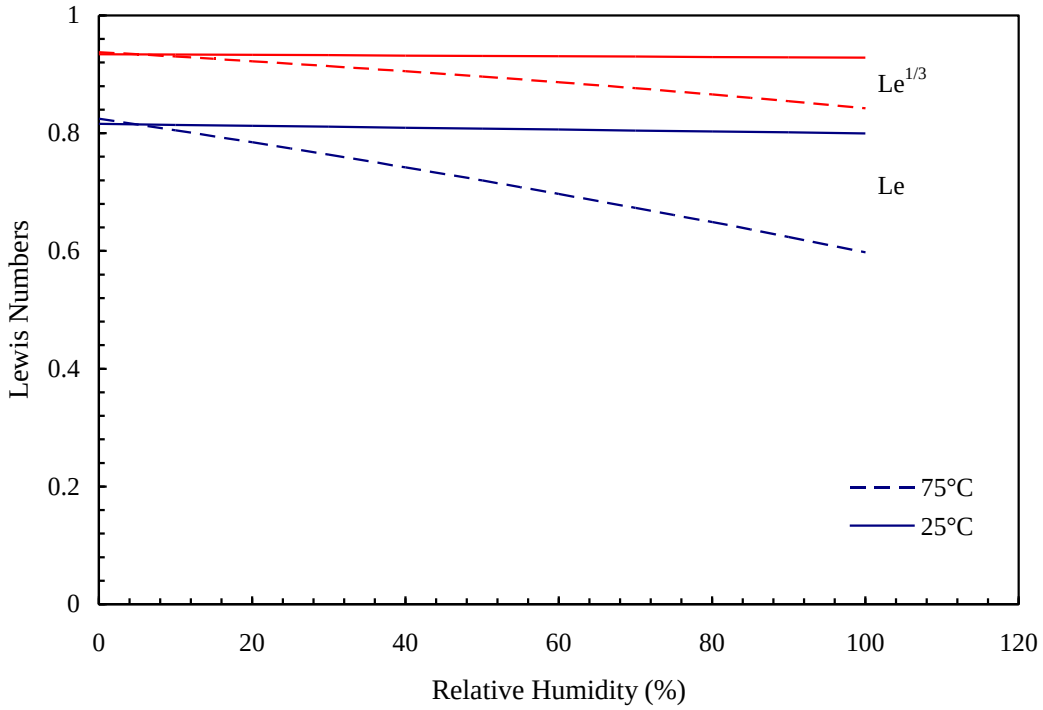


**Figure 3.1:** Variation in Lewis number term with relative humidity at different temperatures

The wet stream of a PEMFC may normally come into the heat and humidity exchanger at around 75°C, whereas in an ERV system the temperatures are closer to 25°C. At 75°C, the value of $Le^{1/3}$ at 100% relative humidity is 10.2% lower compared to that of a stream at 0% relative humidity. This error will then be passed on to the mass transfer coefficient as per Eqn. (28).

## 3.3. CURRENT LATENT EFFECTIVENESS DERIVATIONS

Niu and Zhang derived a latent effectiveness and number of transfer units ($NTU_L$) which closely resembles the sensible heat effectiveness and number of thermal units (NTU) method commonly used in heat exchanger design. They show that the deduction of effectiveness correlations for moisture is of the same form as sensible effectiveness [29]. Heat and humidity exchangers, such as energy (or enthalpy) recovery ventilators (ERVs) commonly have their effectiveness measured with both sensible energy transfer and latent energy transfer. The same effectiveness measures can be applied to humidifiers used in fuel cell applications due to their similar configurations and operating principles. Sections 3.3 to 3.6 of this chapter comprise a version of the article published in the International Journal of Heat and Mass Transfer [44].

The main assumptions used to derive the mathematical model for use with ERVs are [32]:

1. Vapor diffusion and heat conduction in the two air streams along direction of flow are negligible with respect to vapor convection and energy transport by the bulk flow (valid for large Peclet number, Pe = 2 or greater) [29];
2. Adsorption of water vapor at the membrane interface is in an equilibrium adsorption state at steady state operation;
3. The water diffusivity and heat conductivity through the membrane are constants;
4. The heat of sorption is assumed equal to the heat of vaporization and is a constant at the average temperature and pressure of the overall humidifier streams.

The latent effectiveness $\varepsilon_L$ can be defined as

$$\varepsilon_L = \frac{(\dot{m}c_p)_d(\omega_{di} - \omega_{do})}{(\dot{m}c_p)_{\min}(\omega_{di} - \omega_{wi})} \tag{29}$$

The absolute humidity, $\omega$, is used for latent transfer, where dry-bulb temperature is used in the form corresponding to sensible heat transfer. The latent effectiveness measure isolates the moisture-transferring capacity of the device, compared to either a sensible effectiveness or enthalpy effectiveness [12]. The outlet condition can then be determined by rearranging Eqn. (29).

$$\omega_{do} = \omega_{di} - \varepsilon_L \frac{(\dot{m}c_p)_{\min}}{(\dot{m}c_p)_d}(\omega_{di} - \omega_{wi}) \tag{30}$$

Analogous to the expression for number of thermal units used for heat transfer in heat exchangers, a total number of transfer units for latent heat with overall mass transfer coefficient $U_L$ is defined as

$$\mathrm{NTU}_L = \frac{AU_L}{\dot{m}_{\min}} \tag{31}$$

for the total area of transfer $A$ being equal on both sides. As is done for sensible heat, the latent effectiveness can be determined as a function of $\mathrm{NTU}_L$ and another dimensionless parameter, $R_L = \dot{m}_{\min} / \dot{m}_{\max}$. For unmixed cross flows such as those considered in the current chapter (up to Section 3.7) [28]:

$$\varepsilon_L = 1 - \exp\left[\frac{\exp(-\mathrm{NTU}_L^{0.78} R_L) - 1}{\mathrm{NTU}_L^{-0.22} R_L}\right] \tag{32}$$

Other effectiveness correlations are used for different exchanger configurations [27,28]. Humidifiers employed for use in PEMFC applications will normally be in a counter flow arrangement to maximize efficiency; however a cross-flow configuration will be used in this chapter to maintain a means for comparison with the method used for

ERVs. The latent effectiveness can therefore be substituted into Eqn. (30) to determine the outlet moisture content. The total moisture transfer conductance $U_L$ has been calculated by Niu and Zhang.

When considering mass transfer from the wet side to the dry side, diffusion through the membrane as described by adsorption isotherms can be used to adequately account for the water transport [45]. Based on the membrane water uptake characteristics as described by its sorption curve, the water uptake on the dry side in terms of relative humidity $\phi$ would be:

$$\theta_{md} = \theta_{mw} + \left.\frac{\partial \theta}{\partial \phi}\right|_{mw} \Delta\phi = \theta_{mw} + \left.\frac{\partial \theta}{\partial \phi}\right|_{mw} (\phi_{md} - \phi_{mw}) \tag{33}$$

Water flux through the membrane at steady state is modeled with Fick's First Law for diffusion:

$$\dot{m}_{H_2O} = -D_{wm} \nabla \theta \tag{34}$$

According to assumption 1, Eqn. (34) is reduced to the one-dimensional form:

$$\dot{m}_{H_2O} = -D_{wm} \frac{\partial \theta}{\partial z} = D_{wm} \frac{\theta_{mw} - \theta_{md}}{t_{mem}} \tag{35}$$

Incorporating membrane water uptake characteristics by substituting Eqn. (33) into (35) gives:

$$\dot{m}_{H_2O} = \frac{D_{wm}}{t_{mem}} \left.\frac{\partial \theta}{\partial \phi}\right|_{mw} (\phi_{mw} - \phi_{md}) \tag{36}$$

To obtain the overall mass transfer coefficient $U_L$, the relative humidities must be changed into the driving force of absolute humidity $\omega$, from a linear relation between the two parameters. Substituting the Clausius-Clapeyron equation into the relationship between relative humidity and absolute humidity based on vapor partial pressure, Zhang

and Niu (from Simonson and Besant [30]) arrive at the following relation after substituting for the pressure at standard atmosphere:

$$\frac{\phi}{\omega} = \frac{e^{5294\ /\ T}}{10^{\ 6}} - 1.61\phi \tag{37}$$

The second term on the right hand side is ignored in order to simplify the equation to a linear relationship, assumed to have an effect of less than 5%.

$$\phi = \frac{e^{5294\ /\ T}}{10^{\ 6}}\omega \tag{38}$$

Therefore, Eqn. (36) can now be written in terms of the driving force of absolute humidity.

$$\dot{m}_{H_2O} = \frac{D_{wm}}{t_{mem}} \left.\frac{\partial\theta}{\partial\phi}\right|_{mw} \frac{e^{5294\ /\ T}}{10^{\ 6}} \left(\omega_{mw} - \omega_{md}\right) \tag{39}$$

Assuming steady state operation and equilibrium at the interfaces, the moisture transfer across the membrane can be written in terms of surface mass transfer resistances:

$$\dot{m}_{H_2O} = h_{Mw}\left(\omega_{w} - \omega_{mw}\right) = h_{Md}\left(\omega_{md} - \omega_{d}\right) \tag{40}$$

The unknown absolute humidities at the membrane can then be eliminated from Eqn. (39) by first rearranging Eqn. (40).

$$\omega_{mw} = \omega_{w} - \dot{m}_{H_2O} \ / \ h_{Mw} \tag{41}$$

$$\omega_{md} = \omega_{d} + \dot{m}_{H_2O} \ / \ h_{Md} \tag{42}$$

Setting the moisture diffusive resistance in the membrane

$$\gamma_{m} = \frac{t_{mem}}{D_{wm} \left.\frac{\partial\theta}{\partial\phi}\right|_{mw} \frac{e^{5294\ /\ T}}{10^{\ 6}}} \tag{43}$$

and substituting (41) and (42) into Eqn. (39) and rearranging leads to the water transfer in terms of the difference in absolute humidity as the driving force:

$$\dot{m}_{H_2O} = \left( \frac{1}{h_{Mw}} + \gamma_m + \frac{1}{h_{Md}} \right)^{-1} (\omega_w - \omega_d) \tag{44}$$

Therefore, the overall mass transfer coefficient $U_L$ to be used in Eqn. (31) has been found as

$$U_L = \left( \frac{1}{h_{Mw}} + \gamma_m + \frac{1}{h_{Md}} \right)^{-1} \tag{45}$$

The first and third terms on the right side are the convective mass transfer resistances as produced with the heat-mass transfer analogy, while the middle term, Eqn. (43), is analogous to the conduction resistance in heat transfer.

## 3.4. CURRENT LIMITATIONS OF $\varepsilon$-NTU METHOD FOR MASS TRANSFER

This section discusses the limitations of the $\varepsilon$-NTU method for heat and mass transfer in membrane humidity exchangers as proposed by L.Z. Zhang in [29], specifically in the context of applying the same model to PEMFC heat and humidity exchangers. Two key observations can be made regarding the derivations that call into question the validity of the $\varepsilon$-NTU method being applied to fuel cell humidifiers:

1. The Clausius-Clapeyron reference temperature (used in the value for constant enthalpy of vaporization) is a constant and may be far from the actual operating temperature;
2. At higher temperatures, the absolute humidity calculated without the $1.61\phi$ term in Eqn. (37) will diverge substantially due to the non-linear nature of the saturated water vapor pressure curve.

### 3.4.1. USE OF THE CLAUSIUS-CLAPEYRON SATURATION VAPOR PRESSURE EQUATION

The Clausius-Clapeyron equation is a theoretical expression for the saturation vapor pressure of most liquids [46] and provides a direct relation between saturation pressure and temperature (see next section):

$$P_{sat} = P_{ref} \exp\left(\frac{\Delta H_{vap}}{RT_{ref}}\right) \exp\left(-\frac{\Delta H_{vap}}{RT}\right) \tag{46}$$

The form of Clausius-Clapeyron equation used by Zhang (after Simonson Besant [30]) employs a reference state of 3007 Pa and 297.3 K (24.1°C) and assumes a constant heat of vaporization at that state:

$$P_{sat} = 1.629 \times 10^{11} e^{-5294/T} \tag{47}$$

A result of assuming a constant heat of vaporization is that the error in the equation increases with larger deviations from the reference conditions. Figure 3.2 shows the percent deviation of Eqn. (47) compared to the Hyland-Wexler equation. The well-known Goff-Gratch equation is also shown for a third reference correlation.

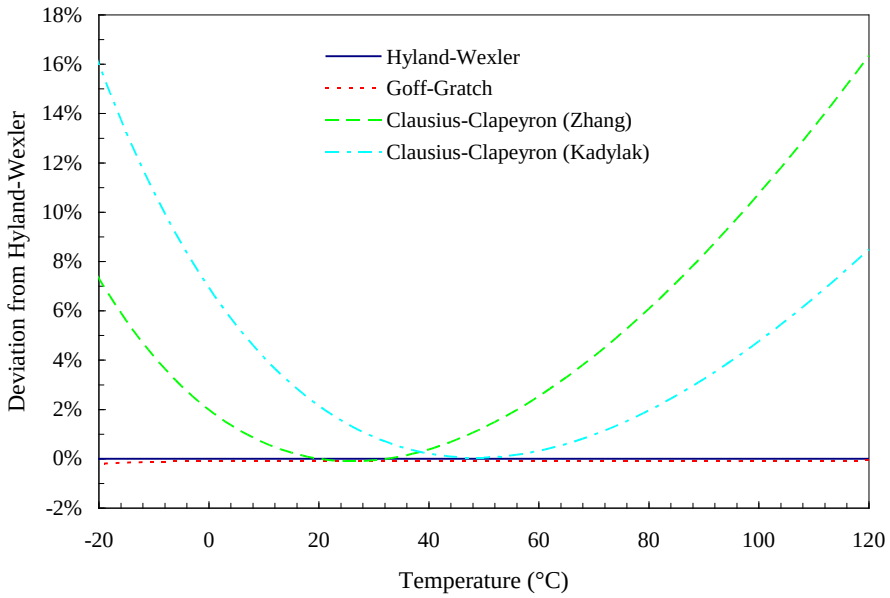


**Figure 3.2:** Comparison of saturated vapor pressure from four different equations

From a survey of fuel cell system manufacturers' requirements for backup and portable power applications, a reference temperature of 50°C is more in line with the operating conditions experienced in PEM fuel cell humidification, and the corresponding heat of vaporization results in a saturation vapor pressure equation in the Clausius-Clapeyron form of:

$$P_{sat} = 7.731 \times 10^{10} e^{-5057/T} \tag{48}$$

The Goff-Gratch and Hyland-Wexler equations show very little deviation from each other and are taken to be most accurate [47], where Goff-Gratch is generally considered the reference equation. The percent deviation of the Clausius-Clapeyron equation used by Zhang, Eqn. (47), is within an acceptable 2% for most atmospheric temperatures, but increases rapidly at either higher or lower temperatures. The Clausius-Clapeyron equation derived for fuel cell applications, Eqn. (48), has also been plotted, and it can be seen that the deviation is within 2% for most fuel cell applications from 21°C to 80°C.

### 3.4.2. CORRELATION BETWEEN ABSOLUTE HUMIDITY AND RELATIVE HUMIDITY

From the definitions of relative humidity and absolute humidity, the following relation can be derived:

$$\frac{\phi}{\omega} = \frac{P}{0.622\ P_{sat}} - \frac{\phi}{0.622} \tag{49}$$

The numeric constant 0.622 is the molecular weight ratio of water to dry air composition. Substituting in Eqn. (47) for a standard atmospheric pressure of 101,325 Pa this time, Zhang (after Simonson and Besant [30]) arrived at:

$$\frac{\phi}{\omega} = \frac{e^{5294\ /\ T}}{10^{\ 6}} - \frac{\phi}{0.622} \tag{50}$$

Zhang (and Simonson and Besant) then neglected the second term on the right hand side on the grounds that it is generally less than 5% of the first term on the right hand side. This approximation can be made if the vapor pressure is much less than the air pressure, and can be arrived at by starting with a simplified version of the definition of humidity ratio.

$$\omega = 0.622\ \frac{P_v}{P - P_v} \approx 0.622\ \frac{P_v}{P},\ P_v << P_{air} \tag{51}$$

While this is a reasonable assumption at atmospheric pressures (~1 atm) and temperatures (20 – 40°C), it is not the case at the higher temperatures that are found in fuel cell humidifiers (see Figure 3.3). With values up to 20% of the other term at 60°C and 100% relative humidity, the second term on the right hand side of Eqn. (50) cannot be neglected. Also, fuel cell operation is not always near atmospheric pressures, so it is premature to substitute the atmospheric pressure into Eqn. (39) at this point.

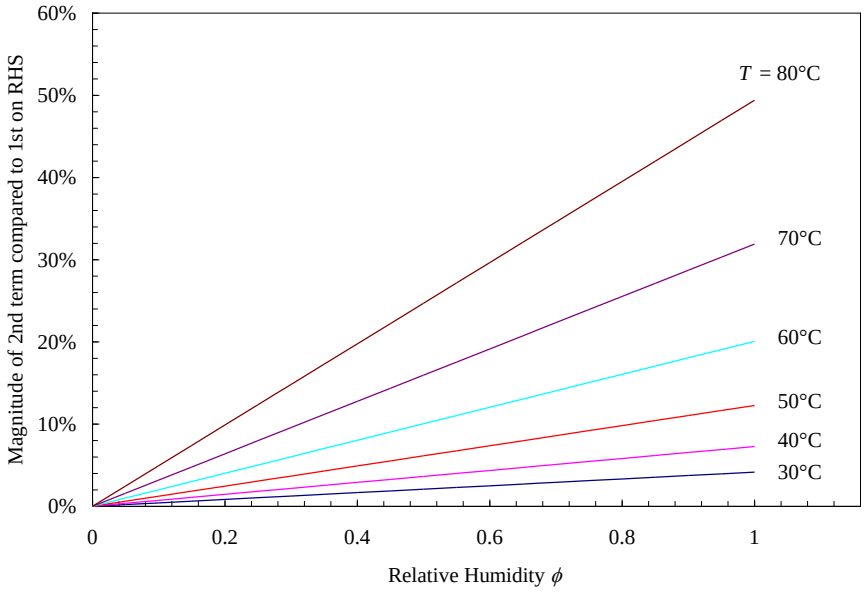


**Figure 3.3:** Magnitude of second term compared to first on right hand side of Eqn. (50)

## 3.5. A NEW APPROACH TO USING LATENT EFFECTIVENESS

This section discusses techniques to address the limitations presented above and to render the $\varepsilon$-NTU method applicable to PEMFC membrane heat and humidity exchangers. Firstly, the Clausius-Clapeyron equation, Eqn. (46), can still be used, but the enthalpy of vaporization and reference states shall be calculated at the operating conditions, and substituted directly into Eqn. (49). As well, the pressure $P$ in Eqn. (49) will remain a variable parameter.

$$\frac{\phi}{\omega} = \frac{P \exp(\Delta H_{vap} / RT)}{0.622\ P_{ref} \exp(\Delta H_{vap} / RT_{ref})} - \frac{\phi}{0.622} \tag{52}$$

The use of the Clausius-Clapeyron equation and neglecting the $\phi$/0.622 term in Eqn. (50) allow Zhang to provide a simplified expression for overall moisture transfer resistance across the membrane analogous to the overall heat transfer coefficient. Without these assumptions, the problem cannot be simplified as easily. The proposed solution is to maintain the $\phi$/0.622 term, thereby making the solution iterative. One has the following system of three flux equations with five unknowns ($J$, $\omega_{mw}$, $\theta_{mw}$, $\omega_{md}$, and $\theta_{md}$):

$$\begin{aligned} J &= h_{Mw}(\omega_w - \omega_{mw}) \\ J &= \frac{D_{wm}}{t_{mem}}(\theta_{mw} - \theta_{md}) \\ J &= h_{Md}(\omega_{md} - \omega_d) \end{aligned} \tag{53}$$

Introducing two more unknowns (relative humidities on either surface of the membrane, $\phi_{md}$ and $\phi_{mw}$) and four equations of relation ($\phi$ to $\omega$ and $\phi$ to $\theta$) close the problem:

$$\begin{aligned} \frac{\phi_{mw}}{\omega_{mw}} &= \frac{P}{0.622\ P_{sat,w}} - \frac{\phi_{mw}}{0.622} \\ \frac{\phi_{md}}{\omega_{md}} &= \frac{P}{0.622\ P_{sat,d}} - \frac{\phi_{md}}{0.622} \end{aligned} \tag{54}$$

where $P_{sat}$ has been left as is, since any saturated water vapor relation can be used, such as the Hyland-Wexler or Goff-Gratch equation referred to in Section 3.4.1.

The two sorption curves for the membrane under consideration, relating water uptake $\theta$ to relative humidity at the membrane interface are the final two equations and can be represented parametrically as:

$$\begin{aligned} \theta_{mw} &= \frac{\theta_{\max}}{1 - C + C/\phi_{mw}} \\ \theta_{md} &= \frac{\theta_{\max}}{1 - C + C/\phi_{md}} \end{aligned} \tag{55}$$

$C$ is a variable denoting the type of membrane being used because the membrane type affects the shape of the sorption curve. A value of $C = 1$ denotes a linear membrane, usually employing a silica gel desiccant. A Type-I membrane such as a molecular sieve has a value of $C < 1$, and Type-III membranes such as those containing polymer desiccants have a value of $C > 1$ [32].

This provides a set of seven equations, two of which are non-linear. Since the problem remains non-linear an iterative approach is required. The proposed solution further requires determining an effective overall mass transfer coefficient $U_{eff}$

$$J = U_{eff}(\omega_w - \omega_d) \tag{56}$$

instead of the overall mass transfer coefficient $U_L$ found through mass transfer resistances in Eqn. (45).

The method of determining the humidifier outputs of absolute humidity is as follows:

- Solve the seven non-linear equations (53) to (55) simultaneously to find the flux $J$;
- Find the effective mass transfer coefficient $U_{eff}$ using Eqn. (56);

- Use $U_{eff}$ in place of $U_L$ in the equation used to find $NTU_L$, Eqn. (31);
- The latent effectiveness is now found from the correlation of Eqn. (32) or similar;
- The outputs can now be found from Eqn. (30).

An outside iterative loop must be implemented involving a first estimate for the outlet values of absolute humidity ($\omega_{do}$ and $\omega_{wo}$), and using subsequent approximations, to obtain values to use for the absolute humidities in Eqn. (56). The process of solving for the outlet conditions is presented in the flow chart of Figure 3.4. The model was created in Mathcad, and the complete details can be found in the Appendix.

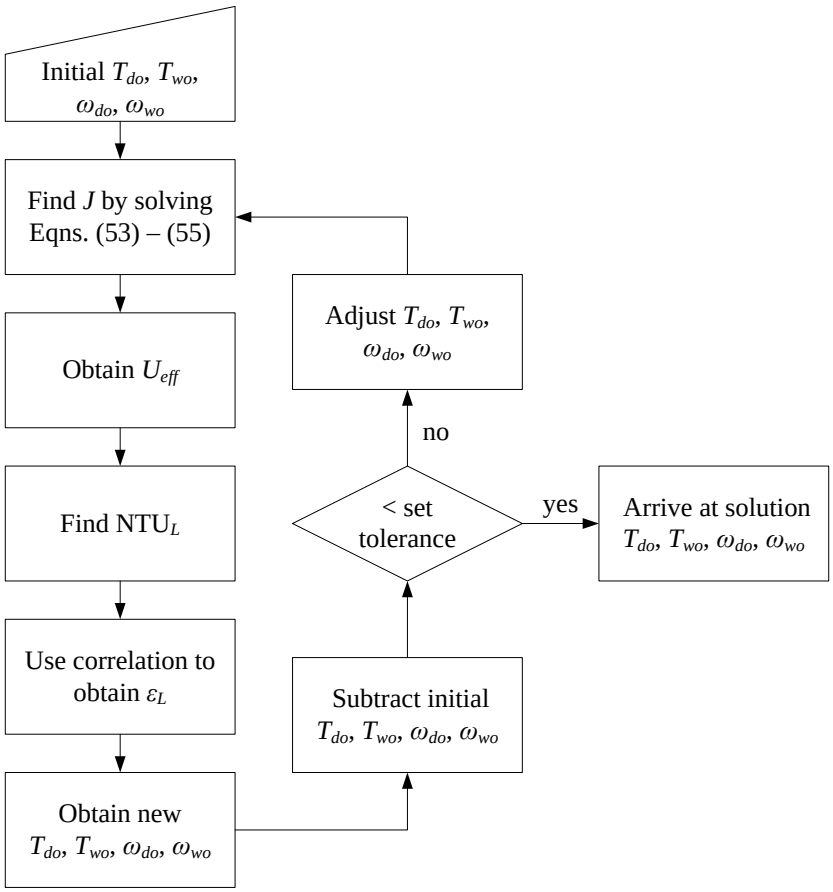


**Figure 3.4:** Procedure for solving humidifier outlet conditions

## 3.6. RESULTS OF COMPARISON TO PREVIOUS EFFECTIVENESS METHOD

The solution presented in the previous section was implemented and compared to the one given by Zhang and Niu. The inputs used for this comparison are summarized in Table 3.1. The inputs were arrived at by considering typical PEM fuel cell conditions but also closely following the parameters used by Zhang and Niu in previous work.

**Table 3.1:** Summary of parameters used in humidifier model comparisons

| | | | | | |
|---|---|---|---|---|---|
| $l$ | 500 | mm | $D_{wm}$ | $2.16 \times 10^{-8}$ | kg/m · s |
| $B$ | 500 | mm | $\theta_{\max}$ | 0.23 | kg/kg |
| $d$ | 5 | mm | membrane | PVC | |
| $w$ | 5 | mm | configuration | cross-flow | |
| $M$ | 30 | layers | $\phi_{di}$ | 0 to 0.9 | RH |
| $n$ | 83 | channels | $\phi_{wi}$ | 1 | RH |
| $\dot{m}$ | 0.05 | kg/s | $T_{di}$ | 70 | °C |
| $Q$ | 2350 | SLPM | $P_{di}$ | 1 | atm |
| $t_{mem}$ | 0.02 | mm | $T_{wi}$ | 70 | °C |
| $k_{mem}$ | 0.18 | W/m · K | $P_{wi}$ | 1 | atm |

Figure 3.5 compares the new method to that used by Zhang and Niu of $NTU_L$ when varying the dry inlet relative humidities from 0 to 90% for three types of membrane. While the new method follows similar trends to that of Zhang and Niu for the corresponding type of membrane, the values in $NTU_L$ vary considerably. The differences are most pronounced for the extreme ranges of dry inlet relative humidities for Type-I and Type-III membranes, and for the higher relative humidities in linear-type membranes.

The effect that a change in $NTU_L$ has on the latent effectiveness is portrayed graphically in Figure 3.6. As expected, the curves of effectiveness follow the same shapes as those for $NTU_L$ for each membrane type. The variations between the two methods employed are of similar magnitude in the $\varepsilon_L$ curves, just as in the $NTU_L$ curves.

According to Eqn. (30) the difference in effectiveness between the two methods will also determine how severely the simplifications made by Zhang and Niu affect the outputs, namely the outlet absolute humidity $\omega_{do}$, when compared to the inlet absolute humidity $\omega_{di}$. Therefore, in an extreme example of 90% relative humidity at the dry inlet for a linear type membrane operating at the 70°C isothermal case investigated (right side of Figure 3.5b), the error caused by using the ERV method would translate to a 40% over-prediction in outlet absolute humidity as compared to the inlet absolute humidity.

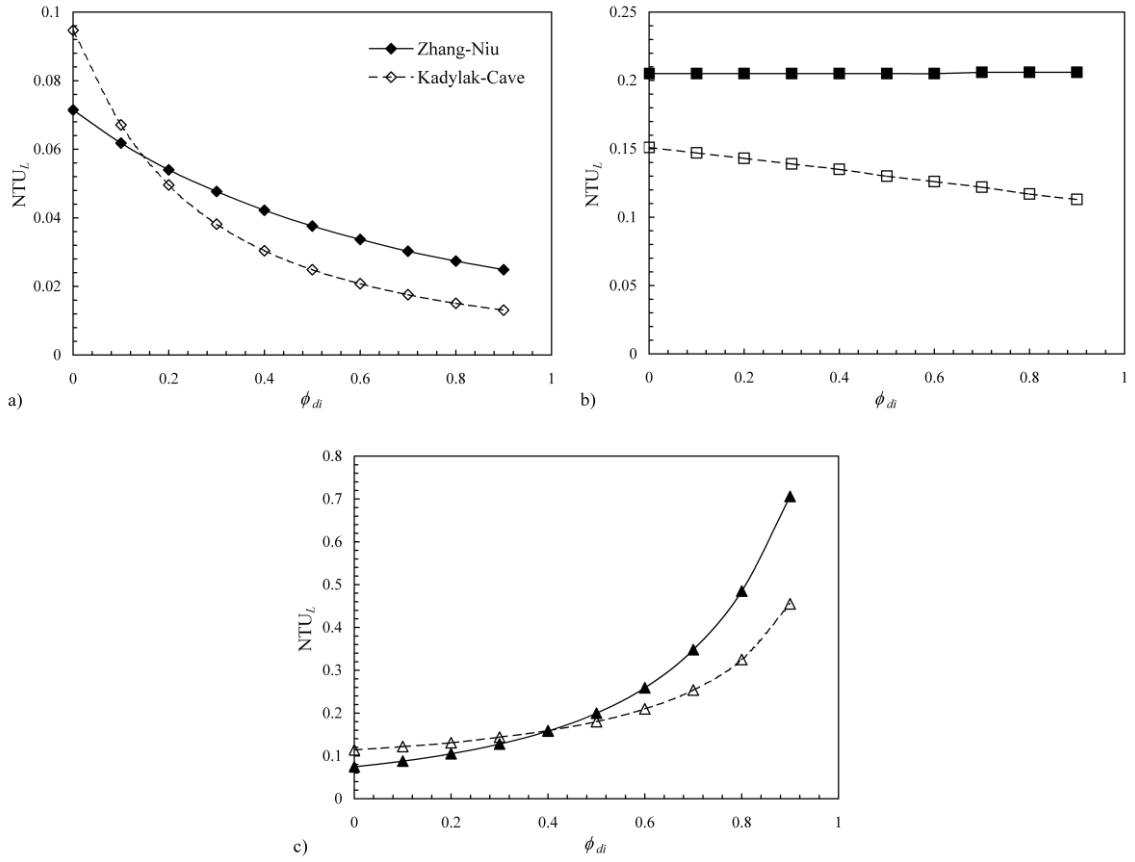


**Figure 3.5:** Variation of $NTU_L$ with inlet relative humidity for constant NTU: a) Type-I membrane ($C$ = 0.1); b) linear-type membrane ($C$ = 1); c) Type-III membrane ($C$ = 10)

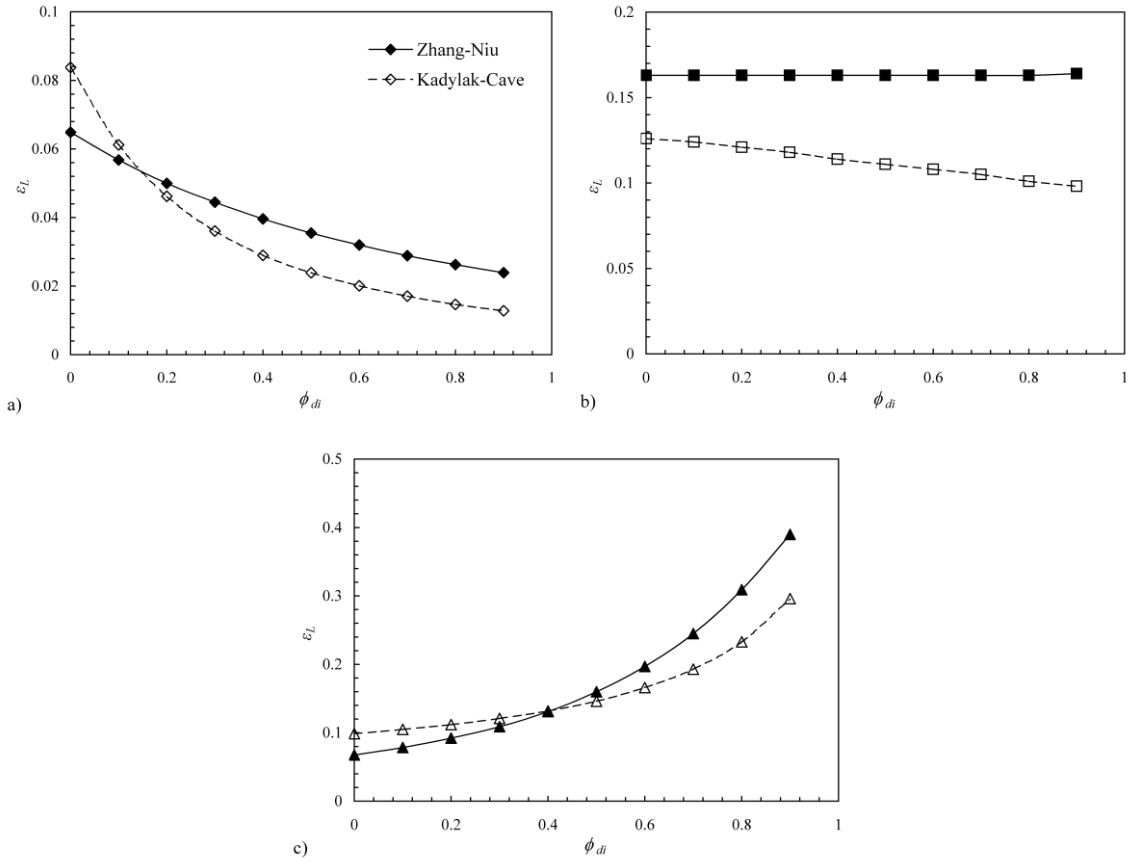


**Figure 3.6:** Latent effectiveness for constant NTU: a) Type-I membrane ($C$ = 0.1); b) linear-type membrane ($C$ = 1); c) Type-III membrane ($C$ = 10)

When dealing with PEMFC humidification, the dry inlet stream will generally be supplied very dry by a compressor or blower creating a dew point of –20°C or lower, or less than 3% relative humidity. Thus, the points of greatest interest on the curves are at the far left, at zero dry inlet relative humidity. Table 3.2 summarizes the $NTU_L$ and latent effectiveness deviations when the simplifications made by Zhang and Niu are used as compared to the proposed solution method of this paper. When the two limitations have been addressed using the new method, improvement is made to the calculated outputs, ranging from 23% to 46% difference if using simplifications in the ERV method, for the Type-III membrane when determining the latent effectiveness for the 70°C isothermal case.

**Table 3.2:** Comparison based on methodology of latent NTU and latent effectiveness for 0% dry inlet RH

| | Difference Kadylak-Cave vs. Zhang-Niu | |
|---|---|---|
| Membrane | $NTU_L$ | $\varepsilon_L$ |
| Type-I | 32.4% | 29.1% |
| linear-type | –26.3% | –22.7% |
| Type-III | 56.8% | 46.4% |

As the conditions for PEMFC operation have larger variations from those of ERVs, it is expected that the difference between effectivenesses found using the two methods will grow, and it will become more important to implement the approach outlined in this chapter. Even for ERV studies, implementing these recommendations will improve outlet condition prediction accuracy.

## 3.7. EXPERIMENTAL VALIDATION OF MODEL

A proper, complete model requires membrane properties to be defined. A diffusion coefficient correlation is the only parameter that remains to be determined; so the diffusion coefficient is treated as a fitted parameter to the data. The temperature chosen to obtain the diffusion coefficient is 25°C, where there is the most confidence in the data. For the polymer-hydrophilic additive membrane, the experimental data point with the least variance occurs at 0.7 SLPM with a standard error of 0.042°C dew point between samples, whereas for the perfluorinated composite membrane the least variance occurs at 0.4 SLPM with a standard error of 3.3°C dew point. The diffusion coefficient for the porous polymer membrane was determined to be $D_m = 9.42 \times 10^{-10}$ m$^2$/s, while for the ionic membrane the diffusion coefficient was found to be $D_m = 6.21 \times 10^{-11}$ m$^2$/s. Although the perfluorinated membrane has a smaller diffusion coefficient by a factor of 15, it performs better in terms of water transfer at equal conditions. As a reference, Chen

and Peng reported the diffusion coefficient for Nafion 115 (0.127 mm thick) to vary between $9.12 \times 10^{-11}$ m$^2$/s and $3 \times 10^{-10}$ m$^2$/s [22].

The diffusion coefficient also needs to be fitted at different temperatures. The diffusion coefficient as a function of temperature is modeled by an Arrhenius relation with activation energy $E_a$, as also found implemented in the literature for Nafion [48]:

$$D_{wm} = D_m \exp\left[\frac{E_a}{R}\left(\frac{1}{T_{ref}} - \frac{1}{T_m}\right)\right] \tag{57}$$

The reference temperature $T_{ref}$ is 298.15 K, the temperature at which $D_m$ was found for the first point. Once the temperature dependence of the diffusion coefficient is applied to the data, as shown in Figure 3.7, the activation energy for the polymer-hydrophilic additive membrane is found to be 24,300 J/mol.

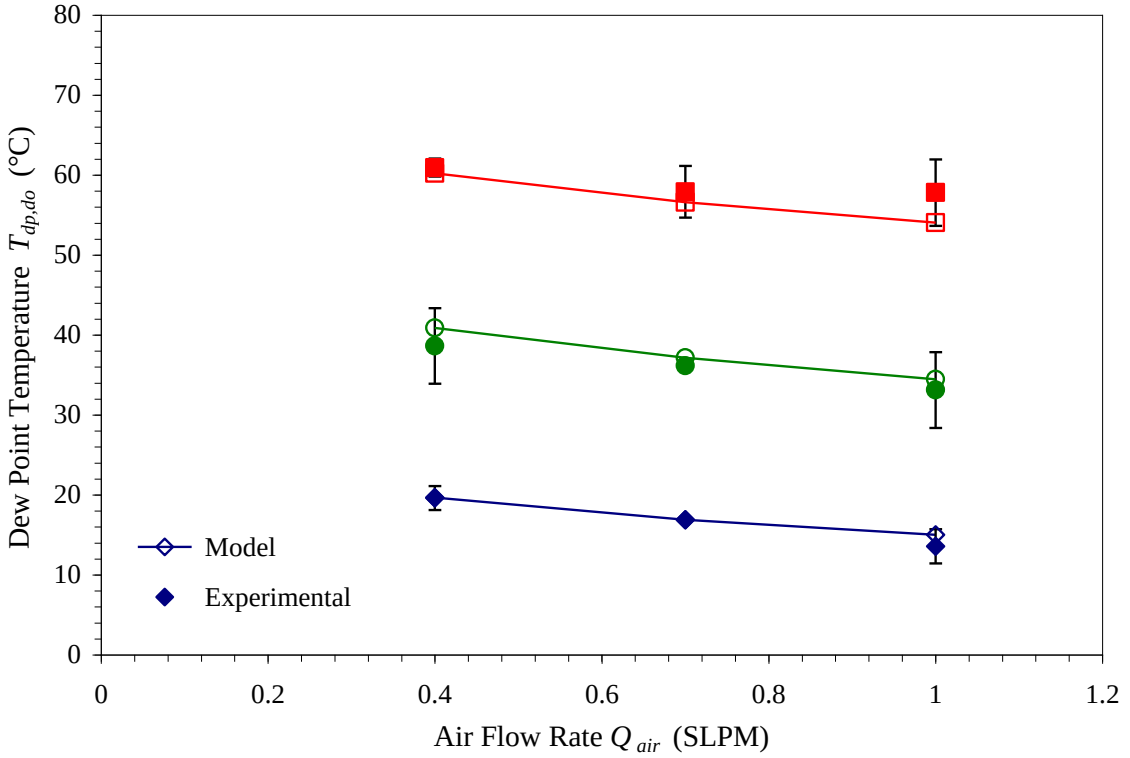


**Figure 3.7:** Model comparison to experimental data for porous polymer with hydrophilic additive membrane, at ♦ $T_{iso}$ = 25°C, ● 50°C, ■ 75°C

Fitting the diffusion coefficient over the range of temperatures for the perfluorinated composite membrane yields an activation energy of 34,800 J/mol, with the results in Figure 3.8. Hence, the model is able to agree with the experimental data to within the experimental error bars corresponding to a 95% confidence interval. Higher activation energy is required for the ionic membrane than for the porous polymer membrane, in order to account for the higher water transfer at high temperatures. The activation energies for these tested membranes are within the vicinity of the activation energies in the literature for Nafion of 20,096 J/mol [48] and 18,003 J/mol [49]. Chen *et al.* also report higher activation energy than Yeo and Eisenberg from their tests with liquid-to-air membrane humidification [19].

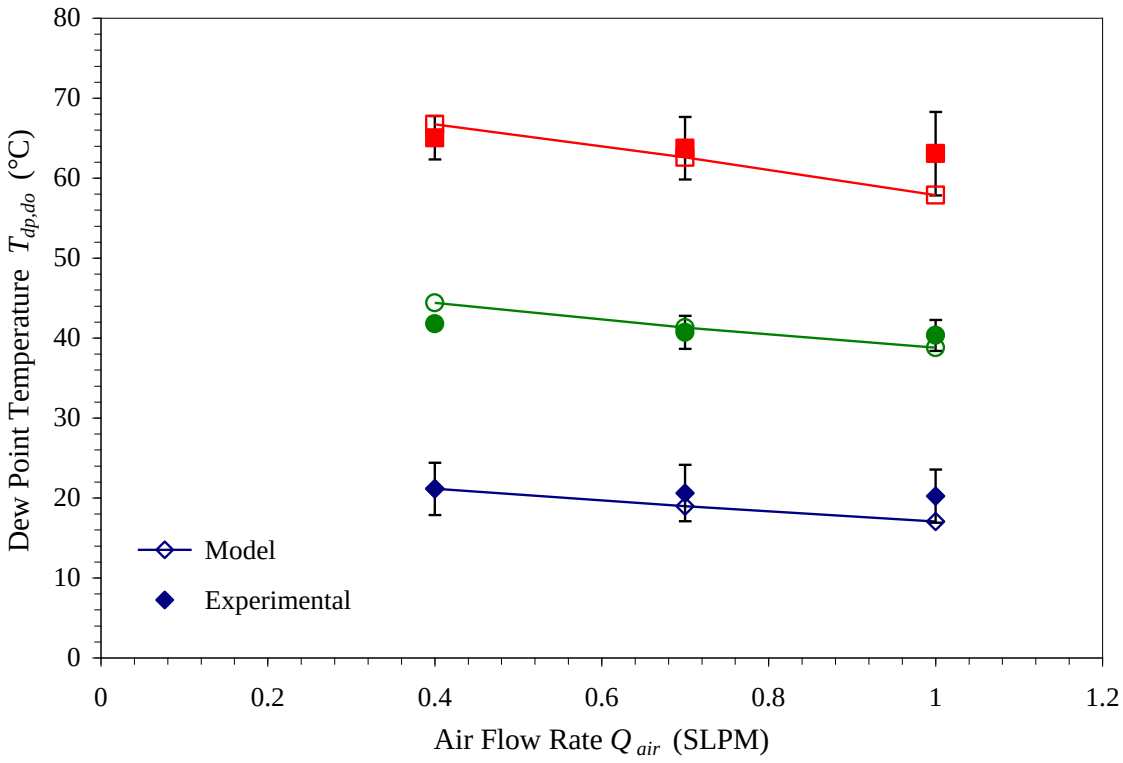


**Figure 3.8:** Model comparison to experimental data for ionic perfluorinated composite membrane, at ♦ 25°C, ● 50°C, ■ 75°C

# 4. CONCLUSIONS

A study on the water transfer performance of humidifiers requires an understanding of different metrics to quantify humidity transfer. Through experiments that varied the parameters that affect water transfer, a key finding was that water recovery ratio is the most appropriate performance metric for fuel cell humidifiers, as it accounts for the amount of water supplied even as the fuel cell operating conditions may change.

Initial experiments demonstrated that temperature has a greater effect on water transport than pressure effects over the practical temperature (25°C – 80°C) and pressure (0 kPag and 120 kPag over 35 kPa pressure difference) operating ranges found in PEM fuel cells. Temperature had three times the effect compared to pressure on the dry outlet dew point temperature in the particular tests conducted on a subscale humidifier.

Membrane characterization experiments revealed that the porous and ionic membranes had similar low water uptake profiles at relative humidities less than 80%, with the profiles increasing sharply after 80%, but the porous membrane had a higher maximum water uptake than the ionic membrane. Conversely, the isothermal experiments conducted in the single cell humidifier with the porous and ionic membranes showed that the ionic composite membrane had better water transport characteristics than the porous polymer-hydrophilic additive membrane, ranging from as low as an 11% improvement at the low temperature, low flow condition up to a 56% improvement at the high flow test condition.

The extension of sensible heat effectiveness-number of transfer units to conditions with latent energy transfer is a method for gauging the enthalpy performance of heat and humidity exchangers. Zhang and Niu have developed a method for determining the latent

effectiveness and latent number of transfer units from an analogy to heat transfer. However, limitations were discovered when applying the technique from ERVs to PEMFC plate-and-frame membrane humidifiers. The two limitations that cause the predicted outlet conditions to deviate from the true conditions are:

1. The use of a constant enthalpy of vaporization taken from a low reference temperature in the Clausius-Clapeyron equation;
2. The simplification used in order to make a linear relationship between relative humidity and absolute humidity.

Using the Clausius-Clapeyron equation with the parameters that Zhang and Niu use will create a 4% deviation from the Hyland-Wexler equation for the water saturation pressure curve at 70°C. With the simplification of the vapor pressure being much less than the air pressure to make the relation between relative humidity and absolute humidity linear, the absolute humidity value from using the relation can be underreported by over a third at 70°C.

Due to the elevated temperatures used in PEM fuel cells as compared to ERV systems and the non-linear dependence of the water saturation curve on temperature, the aforementioned limitations were addressed in order to use the latent effectiveness method for PEMFC membrane humidifiers. This was accomplished by finding an effective mass transfer coefficient $U_{eff}$ instead of the $U_L$ proposed by Zhang and Niu. The $U_{eff}$ coefficient is calculated by first iteratively solving the relevant constitutive equations to find the flux of water through the membrane.

The new procedure was applied to three membrane types (Type I, linear, and Type III) and compared to the curves of latent effectiveness and latent NTU found using Zhang

and Niu's method. In fuel cell operation, the most likely conditions for the incoming wet and dry streams will be 100% and close to 0% relative humidity, respectively. For a 70°C isothermal case, the technique yielded an enhancement in latent effectiveness of 29% for Type-I membranes, 23% for linear-type membranes, and 46% for Type-III membranes as compared to the ERV method.

Since a straightforward thermodynamic model to predict water transport through a membrane was developed, there was also the requirement to validate it with experimental data. Diffusion coefficients were extracted from the experimental data by using an Arrhenius relation for temperature dependence. The porous polymer membrane had a diffusion coefficient of $9.42 \times 10^{-10}$ $m^2/s$, and the ionic perfluorinated membrane had a diffusion coefficient of $6.21 \times 10^{-11}$ $m^2/s$. With the appropriate activation energies in the Arrhenius equation, the model matched the experimental results closely within the 95% confidence interval experimental error bars, thereby validating the practical use of the thermodynamic model for the range of conditions tested.

In conclusion, the key findings put forward in this thesis are:

- Evaluation of performance metrics, identifying water recovery ratio as the most appropriate for fuel cell membrane humidifiers;
- Characterization of the sorption isotherms, water transfer performance, and diffusivity of a porous membrane and an ionic membrane, which had the higher performance;
- Development of a thermodynamic membrane humidifier model amenable to PEM fuel cell conditions based on the heat exchanger effectiveness method; and,

- Corroboration of the heat and mass transfer model with experimental data and correlated diffusion coefficients.

## 4.1. FUTURE WORK

The model is ready to be tested to predict performance of commercially available products, with the caveat that true two-phase flow has not been integrated. As such, it may serve better as a tool to compare the relative performance of two or more humidifiers, or to benchmark the performance of an existing humidifier product. The next steps in further developing the model would be to analyze added complexity, such as accounting for condensation, and thus two-phase flow. Some additions to the model that may prove beneficial would be heat transfer to surroundings and the effect of pressure drop. The effects of pressure difference across the membrane, possibly driving permeation, and the effect of different total pressures—although incorporated into the fluid properties of the flows in the model—could also be investigated. The effect of temperature difference between the two streams, which was not studied because it would introduce condensation and two-phase flow, is another area for further research. The interested researcher is directed to Section 2.2, which lays out the parameters that affect water transfer, for further avenues of investigation that were not covered.

Finally, if different membranes will be used in the model, it is imperative that the membrane be characterized as to its water uptake. Further experiments will need to be undertaken to determine the diffusion coefficient, especially as it relates to temperature.

# REFERENCES


[1] E.J. Carlson, P. Kopf, J. Sinha, S. Sriramulu, Y. Yang, Cost Analysis of PEM Fuel Cell Systems for Transportation, National Renewable Energy Laboratory Report No. NREL/SR-560-39104 (Golden, Colorado) (2005) 85-95.

[2] J. Larminie, A. Dicks, Fuel Cell Systems Explained, second ed., John Wiley & Sons, West Sussex, England, 2003.

[3] N. Rajalakshmi, T.T. Jayanth, R. Thangamuthu, G. Sasikumar, P. Sridhar, K.S. Dhathathreyan. Water transport characteristics of polymer electrolyte membrane fuel cell, Int. J. Hydrogen Energy 29(10) (2004) 1009-1014.

[4] W. Merida, D.A. Harrington, J.M. Le Canut, G. McLean. Characterisation of proton exchange membrane fuel cell (PEMFC) failures via electrochemical impedance spectroscopy, J. Power Sources 161(1) (2006) 264-274.

[5] W. Merida, Diagnosis of PEMFC stack failures via electrochemical impedance spectroscopy, Ph.D. Thesis (2002).

[6] S.D. Knights, K.M. Colbow, J. St-Pierre, D.P. Wilkinson. Aging mechanisms and lifetime of PEFC and DMFC, J. Power Sources 127(1-2) (2004) 127-134.

[7] X. Huang, R. Solasi, Y. Zou, M. Feshler, K. Reifsnider, D. Condit, et al. Mechanical endurance of polymer electrolyte membrane and PEM fuel cell durability, J. Polym. Sci. B 44(16) (2006) 2346-2357.

[8] H. Tang, S. Peikang, S.P. Jiang, F. Wang, M. Pan. A degradation study of Nafion proton exchange membrane of PEM fuel cells, J. Power Sources 170(1) (2007) 85-92.

[9] M.B. Satterfield, J.B. Benziger. Non-Fickian water vapor sorption dynamics by Nafion membranes, J. Phys. Chem. B 112(12) (2008) 3693-3704.

[10] M.B. Satterfield, P.W. Majsztrik, H. Ota, J.B. Benziger, A.B. Bocarsly. Mechanical properties of Nafion and titania/Nafion composite membranes for polymer electrolyte membrane fuel cells, J. Polym. Sci. B 44(16) (2006) 2327-2345.

[11] D.M. Bernardi. Water-balance calculations for solid-polymer-electrolyte fuel cells, J. Electrochem. Soc. 137(11) (1990) 3344-3350.

[12] P. Cave, W. Merida. Water flux in membrane fuel cell humidifiers: flow rate and channel location effects, J. Power Sources 175(1) (2008) 408-418.

[13] R. Huizing, M. Fowler, W. Mérida, J. Dean. Design methodology for membrane-based plate-and-frame fuel cell humidifiers, J. Power Sources 180(1) (2008) 265-275.

[14] F.N. Büchi, S. Srinivasan. Operating proton exchange membrane fuel cells without external humidification of the reactant gases, J. Electrochem. Soc. 144(8) (1997) 2767-2772.

[15] D.P. Wilkinson, H.H. Voss, K. Prater. Water management and stack design for solid polymer fuel cells, J. Power Sources 49(1-3) (1994) 117-127.

[16] Y.A. Çengel, M.A. Boles, Thermodynamics: An Engineering Approach, fourth ed., McGraw-Hill, Boston, 2002.

[17] R.A. Parsons, ASHRAE Handbook: HVAC Systems and Equipment, American Society of Heating, Refrigerating and Air-Conditioning Engineers, Atlanta, Ga., 1996, ch. 42.

[18] P.W. Majsztrik, M.B. Satterfield, A.B. Bocarsly, J.B. Benziger. Water sorption, desorption and transport in Nafion membranes, J. Membr. Sci. 301(1) (2007) 93-106.

[19] D. Chen, W. Li, H. Peng. An experimental study and model validation of a membrane humidifier for PEM fuel cell humidification control, J. Power Sources 180(1) (2008) 461-467.

[20] S. Park, I.-H. Oh. An analytical model of Nafion$^{TM}$ membrane humidifier for proton exchange membrane fuel cells, J. Power Sources 188(2) (2009) 498-501.

[21] S.-K. Park, S.-Y. Choe, S.-H. Choi. Dynamic modeling and analysis of a shell-and-tube type gas-to-gas membrane humidifier for PEM fuel cell applications, Int. J. Hydrogen Energy 33(9) (2008) 2273-2282.

[22] D. Chen, H. Peng. A thermodynamic model of membrane humidifiers for PEM fuel cell humidification control, J. Dyn. Sys., Meas., Control 127(3) (2005) 424-432.

[23] G. Hoogers, Fuel Cell Technology Handbook, CRC Press, Boca Raton, Fla., 2003, p. 4.13.

[24] C.W. Monroe, T. Romero, W. Mérida, M. Eikerling. A vaporization-exchange model for water sorption and flux in Nafion, J. Membr. Sci. 324(1-2) (2008) 1-6.

[25] R. Huizing, Design and membrane selection for gas to gas humidifiers for fuel cell applications, M.A.Sc. Thesis (2007).

[26] P. Cave, Membrane moisture transfer in fuel cell humidifiers, M.A.Sc. Thesis (2007).

[27] W.M. Kays, A.L. London, Compact Heat Exchangers, second ed., McGraw-Hill, New York, 1964.

[28] F.P. Incropera, D.P. DeWitt, Fundamentals of Heat and Mass Transfer, fifth ed., John Wiley & Sons, Toronto, 2002.

[29] L. Zhang, J.L. Niu. Effectiveness correlations for heat and moisture transfer processes in an enthalpy exchanger with membrane cores, J. Heat Transfer 124(5) (2002) 922-929.

[30] C.J. Simonson, R.W. Besant. Energy wheel effectiveness: part I--development of dimensionless groups, Int. J. Heat Mass Transfer 42(12) (1999) 2161-2170.

[31] L. Zhang, Y. Jiang. Heat and mass transfer in a membrane-based energy recovery ventilator, J. Membr. Sci. 163(1) (1999) 29-38.

[32] J.L. Niu, L. Zhang. Membrane-based enthalpy exchanger: material considerations and clarification of moisture resistance, J. Membr. Sci. 189(2) (2001) 179-191.

[33] S.-K. Park, E.A. Cho, I.-H. Oh. Characteristics of membrane humidifiers for polymer electrolyte membrane fuel cells, Korean J. Chem. Eng. 22(6) (2005) 877-881.

[34] Vaisala, Vaisala HUMIDICAP® Humidity and Temperature Transmitter Series HMT330 User's Guide, Vaisala Oyj, Helsinki, 2005, ch. 7.

[35] M. Asaeda, L.D. Du. Separation of alcohol/water gaseous mixtures by thin ceramic membrane, J. Chem. Eng. Jpn. 19(1) (1986) 72-77.

[36] P.W. Gibson. Effect of Temperature on water vapor transport through polymer membrane laminates, Polym. Test. 19(6) (2000) 673-691.

[37] J. Crank, G.S. Park, Diffusion in Polymers, Academic Press, New York, 1968, p. 452.

[38] D.J. Burnett, A.R. Garcia, F. Thielmann. Measuring moisture sorption and diffusion kinetics on proton exchange membranes using a gravimetric vapor sorption apparatus, J. Power Sources 160(1) (2006) 426-430.

[39] C.J. Simonson, R.W. Besant. Energy wheel effectiveness: part II--correlations, Int. J. Heat Mass Transfer 42(12) (1999) 2171-2185.

[40] R.H. Perry, D.W. Green, Perry's Chemical Engineers' Handbook, seventh ed., McGraw-Hill, Toronto, 1997, p. 12.34.

[41] P. Choi, N. Jalani, R. Datta. Thermodynamics and proton transport in Nafion II. Proton diffusion mechanisms and conductivity, J. Electrochem. Soc. 152(3) (2005) 123-130.

[42] T.A.J. Zawodzinski, M. Neeman, L.O. Sillerud, S. Gottesfeld. Determination of water diffusion coefficients in perfluorosulfonate ionomeric membranes, J. Phys. Chem. 95(15) (1991) 6040-6044.

[43] F.M. White, Heat and Mass Transfer, rev. ed., Addison-Wesley, Don Mills, Ontario, 1988, p. 586.

[44] D. Kadylak, P. Cave, W. Merida. Effectiveness correlations for heat and mass transfer in membrane humidifiers, Int. J. Heat Mass Transfer 52(5-6) (2009) 1504-1509.

[45] S.-H. Chen, R.-C. Ruaan, J.-Y. Lai. Sorption and transport mechanism of gases in polycarbonate membranes, J. Membr. Sci. 134(2) (1997) 143-150.

[46] K. Laidler, J. Meiser, Physical Chemistry, Benjamin/Cummings Publishing, Don Mills, Ontario, 1982, ch. 5.2.

[47] C.J. Gibbins. A survey and comparison of relationships for the determination of the saturation vapour pressure over plane surfaces of pure water and of pure ice, Ann. Geophys. 8(12) (1990) 859-885.

[48] S.C. Yeo, A. Eisenberg. Physical properties and supermolecular structure of perfluorinated ion-containing (Nafion) polymers, J. Appl. Polym. Sci. 21(4) (1977) 875-898.

[49] M.W. Verbrugge, E.W. Schneider, R.S. Conell, R.F. Hill. The effect of temperature on the equilibrium and transport properties of saturated poly(perfluorosulfonic acid) membranes, J. Electrochem. Soc. 139(12) (1992) 3421-3428.

[50] J.H. Keenan, J. Kaye, Gas Tables: thermodynamic properties of air, products of combustion and component gases, compressible flow functions, John Wiley & Sons, New York, 1948.

[51] Van Wylen, Gordon John, R.E. Sonntag, C. Borgnakke, Fundamentals of Classical Thermodynamics, fourth ed., John Wiley & Sons, New York, 1994.

# APPENDIX: DOCUMENTED MATHCAD MODEL

[:= assigns a value to a variable or defines a formula]

Highlighted fields are for user inputs.

Apply $\varepsilon$-NTU for heat transfer first.

Define geometry.

| | | |
|---|---|---|
| $l := 135 \cdot mm$ | "average length of channel" | |
| $B := 30 \cdot mm$ | "width of plate" | |
| $w := 3 \cdot mm$ | "width of channel" | |
| $n := 7$ | "number of channels per plate" | |
| $d := 1 \cdot mm$ | "depth or thickness of plate, membrane to membrane" | |
| $M := 2$ | "number of layers or plates" | |
| $A_k := l \cdot B$ | $A_k = 0.004\ m^2$ | |
| $A_{cs} := w \cdot d$ | $A_{cs} = 3 \times 10^{-6}\ m^2$ | "cross-sectional area" |
| $A := w \cdot l$ | $A = 4.05 \times 10^{-4}\ m^2$ | |
| $A_c := A + 2 \cdot l \cdot d$ | $A_c = 6.75 \times 10^{-4}\ m^2$ | "2 ½-walls of each stream" |
| $A_h := A_c$ | $A_h = 6.75 \times 10^{-4}\ m^2$ | "equal heat transfer areas" |
| $P_{wet} := 2 \cdot (w + d)$ | $P_{wet} = 0.008\ m$ | "wetted perimeter" |
| $D_h := \frac{4 \cdot A_{cs}}{P_{wet}}$ | $D_h = 1.5\ mm$ | "hydraulic diameter" |

Membrane properties (for porous polymer with hydrophilic additive) and characteristics.

| | | |
|---|---|---|
| $t_{mem} := 0.18\ mm$ | $\rho_{mem} := 0.7 \cdot 940 \cdot kg/m^3$ | $k_{mem} := 0.48 \cdot W/m \cdot K$ |

Sorption curve for porous polymer with hydrophilic additive, PFSA coated both sides:

$C := 148$ $u_{max} := 2.5$ $\phi := 0.005, 0.01..1$

$$G := \begin{pmatrix} 0.0014 \\ 0.1793 \\ -0.37 \\ 0.318 \end{pmatrix}$$ "coefficients for third-degree polynomial fit of sorption curve"

$$u(\phi) := if\left(\phi > 1, u_{max}, if\left(\phi > 0.8, \frac{u_{max}}{1 - C + C/\phi}, G_1 + G_2 \cdot \phi + G_3 \cdot \phi^2 + G_4 \cdot \phi^3\right)\right)$$

Diffusion coefficient will be fitted to one test run at one flow rate and checked vs. rest.

$D_m := 9.42 \cdot 10^{-10} \cdot m^2/s$

Air properties at 1 atm [50]:

[create look-up matrices of temperature $T_{air}$ (1 atm·K/1 bar) and enthalpy $h_{air}$ (J/kg)]

$h_a(temp) := linterp(T_{air}, h_{air}, temp)$ "Mathcad function to interpolate enthalpy"

$$\rho_{air}(P,T) := \frac{P}{(287.05 \cdot J/kg \cdot K) \cdot T}$$ "ideal gas state equation for density"

$$c_{pair}(T) := \left[2.67 \cdot 10^{-6} \cdot \left(\frac{T}{K}\right)^3 - 0.0022 \cdot \left(\frac{T}{K}\right)^2 + 0.623 \cdot \left(\frac{T}{K}\right) + 946\right] \cdot \frac{J}{kg \cdot K}$$

$$\mu_{air}(T) := \left[-3.1 \cdot 10^{-11} \cdot \left(\frac{T}{K}\right)^2 + 6.717 \cdot 10^{-8} \cdot \left(\frac{T}{K}\right) + 1.103 \cdot 10^{-6}\right] \cdot \frac{N \cdot s}{m^2}$$

$$k_{air}(T) := \left[5.333 \cdot 10^{-10} \cdot \left(\frac{T}{K}\right)^3 - 5.4 \cdot 10^{-7} \cdot \left(\frac{T}{K}\right)^2 + 2.557 \cdot 10^{-4} \cdot \left(\frac{T}{K}\right) - 0.0162\right] \cdot \frac{W}{m \cdot K}$$

$$\alpha_{air}(T) := \left[1.4 \cdot 10^{-10} \cdot \left(\frac{T}{K}\right)^2 + 5.1 \cdot 10^{-8} \cdot \left(\frac{T}{K}\right) - 5.8 \cdot 10^{-6}\right] \cdot \frac{m^2}{s}$$

Saturated water properties at 1 bar [51]:

[create look-up matrices of temperature $T$ (°C); pressure $P$ (Pa); liquid enthalpy $h_f$ (J/kg); enthalpy of evaporation $h_{fg}$ (J/kg); vapor density $\rho_v$ (kg/m$^3$); liquid density $\rho_l$ (kg/m$^3$)]

$P_{sat}(temp) := linterp(T,P,temp)$ $T_{sat}(press) := linterp(P,T,press)$

$h_w(temp) := linterp(T,h_f,temp)$ $h_v(temp) := linterp(T,h_{fg},temp)$

$h_g(temp) := h_w(temp) + h_v(temp)$ $\rho_g(temp) := linterp(T, \rho_v,temp)$

$$c_{pg}(T) := \left[ -1.778 \cdot 10^{-9} \cdot \left(\frac{T}{K}\right)^3 + 2.952 \cdot 10^{-6} \cdot \left(\frac{T}{K}\right)^2 - 0.001039 \cdot \left(\frac{T}{K}\right) + 1.958 \right] \cdot \frac{J}{kg \cdot K}$$

$$\mu_g(T) := \left[ 3.608 \cdot 10^{-8} \cdot \left(\frac{T}{K}\right) - 9.933 \cdot 10^{-7} \right] \cdot \frac{N \cdot s}{m^2}$$

$$k_g(T) := \left[ 2.1695 \cdot 10^{-5} \cdot \left(\frac{T}{K}\right)^{1.18362} \right] \cdot \frac{W}{m \cdot K}$$

$$\alpha_g(T) := \left[ -1.43 \cdot 10^{-12} \cdot \left(\frac{T}{K}\right)^2 + 1.264 \cdot 10^{-9} \cdot \left(\frac{T}{K}\right) - 1.038 \cdot 10^{-7} \right] \cdot \frac{m^2}{s}$$

Cold and hot stream flow rates.

$Q_c := \frac{0.4}{n} \cdot \frac{L}{min} \cdot \frac{2}{M}$ $Q_c = 9.5238 \times 10^{-7} \cdot \frac{m^3}{s}$ “cold (dry) side flow rate”

$m'_c := \rho_{air}(1 \cdot atm, 273.15 \cdot K) \cdot Q_c$ $m'_c = 1.2307 \times 10^{-6}$ kg/s “at STP”

$Q_h := Q_c$ $Q_h = 9.5238 \times 10^{-7} \cdot \frac{m^3}{s}$ “hot (wet) side flow rate”

$m'_h := \rho_{air}(1 \cdot atm, 273.15 \cdot K) \cdot Q_h$ $m'_h = 1.2307 \times 10^{-6}$ kg/s “at STP”

First guess for use in dry (cold) fluid properties, iteratively adjust cyan highlighted values.

$T_1 := 75$ °C $P_1 := 1 \cdot atm$ “absolute” $\phi_1 := 0.0016$ “known inputs”

$T_2 := 75$ °C $P_2 := 1 \cdot atm$ “absolute” $\phi_2 := 0.508$ “first guesses”

Converting given conditions to humidity ratio.

$$\omega_1 := \frac{0.622 \cdot \phi_1 \cdot P_{sat}(T_1)}{P_1 - \phi_1 \cdot P_{sat}(T_1)} \qquad \omega_1 = 3.7914 \times 10^{-4} \text{ “kg water/kg dry air”}$$

$$\omega_1 := \frac{0.622 \cdot \phi_2 \cdot P_{sat}(T_2)}{P_2 - \phi_2 \cdot P_{sat}(T_2)} \qquad \omega_2 = 0.1492 \text{ “kg water/kg dry air”}$$

Work out average properties of humid air for dry (“cold”) side.

$$\phi_c := \min\left(1, \frac{\phi_1 + \phi_2}{2}\right) \qquad \phi_c = 0.2548 \qquad \text{“average RH based on inlet 1 and outlet 2”}$$

$$T_c := \frac{T_1 + T_2}{2} \qquad T_c = 75\ ^\circ\text{C} \qquad \text{“average temperature of dry (cold) stream”}$$

$$P_c := \frac{P_1 + P_2}{2} \qquad P_c = 1.0132 \times 10^5 \text{ Pa} \quad \text{“average pressure of dry stream”}$$

$$P_{vc} := \phi_c \cdot P_{sat}(T_c) \qquad P_{vc} = 9829.6744 \text{ Pa} \qquad \text{“vapor pressure of dry (cold) stream”}$$

$$\omega_c := \frac{0.622 \cdot P_{vc}}{P_c - P_{vc}} \qquad \omega_c = 0.0668 \text{ “kg water/kg dry air”}$$

$$x_c := \frac{\omega_c}{1 + \omega_c} \qquad x_c = 0.0626 \qquad \text{“mass fraction of water vapor”}$$

$$\rho_c := \frac{P_c}{1 \cdot \text{atm}} \left( \frac{x_c}{\rho_g(T_c)} + \frac{1 - x_c}{\rho_{air}(P_c, T_c)} \right)^{-1} \qquad \rho_c = 0.8451 \ \frac{\text{kg}}{\text{m}^3}$$

$$c_{pc} := x_c \cdot c_{pg}(T_c) + (1 - x_c) \cdot c_{pair}(T_c) \qquad c_{pc} = 945.8311 \text{ J/kg·K}$$

$$\mu_c := x_c \cdot \mu_g(T_c) + (1 - x_c) \cdot \mu_{air}(T_c) \qquad \mu_c = 2.0157 \times 10^{-5} \text{ kg/s·m}$$

$$k_c := x_c \cdot k_g(T_c) + (1 - x_c) \cdot k_{air}(T_c) \qquad k_c = 0.0294 \text{ W/m·K}$$

$$\alpha_c := x_c \cdot \alpha_g(T_c) + (1 - x_c) \cdot \alpha_{air}(T_c) \qquad \alpha_c = 2.7123 \times 10^{-5} \text{ m}^2/\text{s}$$

$$D_{ABc} := \left(2.3 \cdot 10^{-5} \cdot \frac{\text{m}^2}{\text{s}}\right) \cdot \left(\frac{1 \cdot \text{atm}}{P_c}\right) \cdot \left(\frac{T_c}{273.15 \cdot \text{K}}\right)^{1.74} \qquad D_{ABc} = 3.508 \times 10^{-5} \ \frac{\text{m}^2}{\text{s}} \qquad \text{from [43]}$$

$\mathrm{Re}_c := \frac{m'_c \cdot D_h}{A_{cs} \cdot \mu_c}$ $\mathrm{Re}_c = 30.5293$ "Re < 2300, therefore laminar flow"

First guess for use in wet (hot) fluid properties, iteratively adjust cyan highlighted values.

$T_3 := 75\ °C$ $P_3 := 1 \cdot atm$ "absolute" $\phi_3 := 1$ "known inputs"

$T_4 := 75\ °C$ $P_4 := 1 \cdot atm$ "absolute" $\phi_4 := 0.647$ "first guesses"

Converting given conditions to humidity ratio.

$\omega_3 := \frac{0.622 \cdot \phi_3 \cdot P_{sat}(T_3)}{P_3 - \phi_3 \cdot P_{sat}(T_3)}$ $\omega_3 = 0.3824$ "kg water/kg dry air"

$\omega_4 := \frac{0.622 \cdot \phi_4 \cdot P_{sat}(T_4)}{P_4 - \phi_4 \cdot P_{sat}(T_4)}$ $\omega_4 = 0.2033$ "kg water/kg dry air"

Work out average properties of humid air for wet ("hot") side.

$\phi_h := \min\left(1, \frac{\phi_3 + \phi_4}{2}\right)$ $\phi_h = 0.8235$ "average RH based on inlet 3 and outlet 4"

$T_h := \frac{T_3 + T_4}{2}$ $T_h = 75\ °C$ "average temperature of wet (wet) stream"

$P_h := \frac{P_3 + P_4}{2}$ $P_h = 1.0132 \times 10^5\ Pa$ "average pressure of wet stream"

$P_{vh} := \phi_h \cdot P_{sat}(T_h)$ $P_{vh} = 3.1769 \times 10^4\ Pa$ "vapor pressure of wet (hot) stream"

$\omega_h := \frac{0.622 \cdot P_{vh}}{P_h - P_{vh}}$ $\omega_h = 0.2841$ "kg water/kg dry air"

$x_h := \frac{\omega_h}{1 + \omega_h}$ $x_h = 0.2212$ "mass fraction of water vapor"

$\rho_h := \frac{P_h}{1 \cdot atm}\left(\frac{x_h}{\rho_g(T_h)} + \frac{1 - x_h}{\rho_{air}(P_h, T_h)}\right)^{-1}$ $\rho_h = 0.5946\ \frac{kg}{m^3}$

$c_{ph} := x_h \cdot c_{pg}(T_h) + (1 - x_h) \cdot c_{pair}(T_h)$ $c_{ph} = 786.1145\ J/kg \cdot K$

$\mu_h := x_h \cdot \mu_g(T_h) + (1 - x_h) \cdot \mu_{air}(T_h)$ $\mu_h = 1.8704 \times 10^{-5}$ kg/s·m

$k_h := x_h \cdot k_g(T_h) + (1 - x_h) \cdot k_{air}(T_h)$ $k_h = 0.0282$ W/m·K

$\alpha_h := x_h \cdot \alpha_g(T_h) + (1 - x_h) \cdot \alpha_{air}(T_h)$ $\alpha_h = 2.2562 \times 10^{-5}$ m$^2$/s

$$D_{ABh} := \left(2.3 \cdot 10^{-5} \cdot \frac{\mathrm{m}^2}{\mathrm{s}}\right) \cdot \left(\frac{1 \cdot \mathrm{atm}}{P_h}\right) \cdot \left(\frac{T_h}{273.15 \cdot \mathrm{K}}\right)^{1.74} \quad D_{ABh} = 3.508 \times 10^{-5} \frac{\mathrm{m}^2}{\mathrm{s}}$$ from [43]

$$\mathrm{Re}_h := \frac{m'_h \cdot D_h}{A_{cs} \cdot \mu_h}$$ $\mathrm{Re}_h = 32.9013$ "Re < 2300, therefore laminar flow"

For laminar, fully developed flow and uniform surface heat flux (not uniform surface temperature), Nusselt number Nu is constant, and for a channel of aspect ratio *w*/*d* the heat transfer coefficient is given by [43]:

$$h_c := \left[-0.0391 \cdot \left(\frac{w}{d}\right)^2 + 0.772 \cdot \left(\frac{w}{d}\right) + 2.82\right] \cdot \frac{k_c}{D_h} \quad h_c = 93.7316 \ \frac{\mathrm{W}}{\mathrm{m}^2 \cdot \mathrm{K}}$$

(Assumes heat flux from all walls surrounding cold channels.)

$$h_h := \left[-0.0391 \cdot \left(\frac{w}{d}\right)^2 + 0.772 \cdot \left(\frac{w}{d}\right) + 2.82\right] \cdot \frac{k_h}{D_h} \quad h_h = 89.8109 \ \frac{\mathrm{W}}{\mathrm{m}^2 \cdot \mathrm{K}}$$

(Not much different than $h_c$, so it is assumed that $T_4$ is not important.)

For the side-walls of the ribs treated as fins [27,28]:

$t_{rib} := 1.5 \cdot \mathrm{mm}$ "thickness/width of ribs (lands)"

$$m_{fc} := \left[\frac{2 \cdot h_c \cdot (t_{rib} + l)}{k_{mem} \cdot (t_{rib} \cdot l)}\right]^{0.5} \quad m_{fc} = 513.0873 \ \frac{1}{\mathrm{m}}$$

$$\eta_{fc} := \frac{\tanh(0.5 \cdot m_{fc} \cdot d)}{0.5 \cdot m_{fc} \cdot d}$$ $\eta_{fc} = 0.9786$ "dry fin efficiency"

$$m_{fh} := \left[\frac{2 \cdot h_h \cdot (t_{rib} + l)}{k_{mem} \cdot (t_{rib} \cdot l)}\right]^{0.5} \quad m_{fh} = 502.2415 \ \frac{1}{\mathrm{m}}$$

$$\eta_{fh} := \frac{\tanh(0.5 \cdot m_{fh} \cdot d)}{0.5 \cdot m_{fh} \cdot d} \qquad \eta_{fh} = 0.9795 \qquad \text{“wet fin efficiency”}$$

The temperature ineffectiveness of an extended surface area is found from:

$$\eta_{oc} := 1 - \frac{(n-1) \cdot 2 \cdot l \cdot d}{n \cdot A_c} \cdot (1 - \eta_{fc}) \qquad \eta_{oc} = 0.9786 \qquad \text{“overall efficiency”}$$

$$\eta_{oh} := 1 - \frac{(n-1) \cdot 2 \cdot l \cdot d}{n \cdot A_h} \cdot (1 - \eta_{fh}) \qquad \eta_{oh} = 0.993 \qquad \text{“overall efficiency”}$$

The overall heat transfer $U$ coefficient is then:

$$U := \left( \frac{1}{\eta_{oc} \cdot h_c} + \frac{t_{mem} \cdot A_c}{k_{mem} \cdot A_k} \cdot \frac{A_c}{A_h \cdot \eta_{oh} \cdot h_h} \right)^{-1} \qquad U = 45.4063 \ \frac{\text{W}}{\text{m}^2 \cdot \text{K}}$$

(Not much different from $0.5h$, so membrane conductivity $k_{mem}$ is negligible.)

This is for a gas to gas heat exchanger and specific heat of air does not change much, so the heat capacity rates $C_c$ and $C_h$ are close to the same [28].

$C_c := m'_c \cdot c_{pc}$ $\qquad$ $C_h := m'_h \cdot c_{ph}$

$C_{\min} := \min(C_c, C_h)$ $\qquad$ $C_{\min} = 9.6751 \times 10^{-4}$ m$^2$·kg/K·s$^3$

$C_{\max} := \max(C_c, C_h)$ $\qquad$ $C_{\max} = 0.0012$ m$^2$·kg/K·s$^3$

$$\text{NTU} := \frac{U \cdot A_c}{C_{\min}} \qquad \text{NTU} = 31.6786$$

$$C_r := \frac{C_{\min}}{C_{\max}} \qquad C_r = 0.8311$$

Assuming that the effectiveness relation for plate and frame is the same as for concentric tube heat exchangers, then for counter flow [27,28]:

$$\varepsilon := if\left[ C_r = 1, \frac{\text{NTU}}{1 + \text{NTU}}, \frac{1 - \exp[-\text{NTU} \cdot (1 - C_r)]}{1 - C_r \cdot \exp[-\text{NTU} \cdot (1 - C_r)]} \right] \qquad \varepsilon = 0.9992$$

$q := \varepsilon \cdot C_{\min} \cdot (T_3 - T_1)$ $\qquad$ $q = 0$ W $\qquad$ “heat transfer”

$T_2 := T_1 + \frac{q}{C_c}$ $\underline{T_2 = 75\ °C}$ "converge with initial value"

$T_4 := T_3 - \frac{q}{C_h}$ $\underline{T_4 = 75\ °C}$ "converge with initial value"

The pinch point, or dry bulb approach temperature, is:

$DBAT := T_3 - T_2$ $DBAT = 0\ K$

Apply the $\varepsilon_L$-$NTU_L$ method for latent (moisture) transfer.

Using the Chilton-Colburn Analogy to find the dry and wet mass transfer coefficients $h_M$, where Le = $\alpha/D_{AB}$:

$h_{Mc} := \frac{h_c}{c_{pc}} \cdot \left(\frac{\alpha_c}{D_{ABc}}\right)^{1/3}$ $h_{Mc} = 0.091\ \frac{kg}{s \cdot m^2}$

$h_{Mh} := \frac{h_h}{c_{ph}} \cdot \left(\frac{\alpha_h}{D_{ABh}}\right)^{1/3}$ $h_{Mh} = 0.0986\ \frac{kg}{s \cdot m^2}$ "relatively similar result to $h_{Mc}$"

$T_m := \frac{T_c + T_h}{2}$ $T_m = 348.15\ K$ "assume average membrane temp."

$\phi_m := \frac{\phi_c + \phi_h}{2}$ $\phi_m = 0.5392$ "average membrane water content"

$\omega_m := \frac{\omega_c + \omega_h}{2}$ $\omega_{mh} := \omega_h$ $\omega_{mc} := \omega_c$

Since the gradient in the flux equation is uptake (kg water/kg membrane), need to multiply diffusion coefficient by $\rho_{mem}$:

$E_a := 24300 \cdot J/mol$ $R := 8.3145 \cdot J/mol \cdot K$

$D_{wm} := \rho_{mem} \cdot D_m \cdot \exp\left[\frac{E_a}{R}\left(\frac{1}{298.15 \cdot K} - \frac{1}{T_m}\right)\right]$ $D_{wm} = 2.5332 \times 10^{-6}\ \frac{kg}{s \cdot m}$

Initialize variables for solver:

$\phi_{mc} := 0.1$ $\phi_{mh} := 0.9$ $J := h_{mh}\cdot(\omega_h - \omega_{mh})$ $J = 0\ \text{kg/s}\cdot\text{m}^2$

$u_{mc} := \frac{u_{max}}{1 - C + C/\phi_{mc}}$ $u_{mc} = 0.0019$ $u_{mh} := \frac{u_{max}}{1 - C + C/\phi_{mh}}$ $u_{mh} = 0.1433$

*Given*

$J - h_{mc}\cdot(\omega_c - \omega_{mc}) = 0$ $J - D_{wm}\cdot(u_{mh} - \omega_{mc})/t_{mem} = 0$ $J - h_{mh}\cdot(\omega_{mh} - \omega_h) = 0$

$$\frac{\phi_{mc}}{\omega_{mc}} - \left( \frac{P_c}{0.622 \cdot P_{sat}(T_c)} - \frac{\phi_{mc}}{0.622} \right) = 0 \qquad \frac{\phi_{mh}}{\omega_{mh}} - \left( \frac{P_h}{0.622 \cdot P_{sat}(T_h)} - \frac{\phi_{mh}}{0.622} \right) = 0$$

$u_{mc} - u(\phi_{mc}) = 0$ $u_{mh} - u(\phi_{mh}) = 0$

$$\begin{pmatrix} J' \\ \omega'_{md} \\ \phi'_{md} \\ u'_{md} \\ \omega'_{mw} \\ \phi'_{mw} \\ u'_{mw} \end{pmatrix} := Find\left(J, \omega_{mc}, \phi_{mc}, u_{mc}, \omega_{mh}, \phi_{mh}, u_{mh}\right) \qquad \begin{pmatrix} \omega'_{md} \\ \phi'_{md} \\ u'_{md} \\ \omega'_{mw} \\ \phi'_{mw} \\ u'_{mw} \end{pmatrix} = \begin{pmatrix} 0.2782 \\ 0.8117 \\ 0.0707 \\ 0.0732 \\ 0.2766 \\ 0.0294 \end{pmatrix}$$

Check: $J - h_{mh}\cdot(\omega_h - \omega_{mh}) = 0\ \text{kg/m}^2\cdot\text{s}$ $J' = 5.8168 \times 10^{-4}\ \text{kg/m}^2\cdot\text{s}$

The effective overall mass transfer coefficient $U_{eff}$ according to the new method is then:

$U_{eff} := \frac{J'}{\omega_h - \omega_c}$ $U_{eff} = 0.0027\ \frac{\text{kg}}{\text{m}^2\cdot\text{s}}$

$m'_{min} := \min(m'_c, m'_h)$ $m'_{min} = 1.231 \times 10^{-6}\ \text{kg/s}$

$m'_{max} := \max(m'_c, m'_h)$ $m'_{max} = 1.231 \times 10^{-6}\ \text{kg/s}$

$NTU_L := \frac{A \cdot U_{eff}}{m'_{min}}$ $NTU_L = 0.881$ $R_L := \frac{m'_{min}}{m'_{max}}$ $R_L = 1$

Latent effectiveness:

$$\varepsilon_L := if\left[ R_L = 1, \frac{NTU_L}{1 + NTU_L}, \frac{1 - \exp[-NTU_L \cdot (1 - R_L)]}{1 - R_L \cdot \exp[-NTU_L \cdot (1 - R_L)]} \right] \qquad \varepsilon_L = 0.4684$$

$\omega_2 := \omega_1 + \varepsilon_L \cdot \frac{C_{min}}{C_c} \cdot (\omega_3 - \omega_1)$ $\omega_2 = 0.1491$ "kg water/kg dry air"

$\omega_4 := \omega_3 + \varepsilon_L \cdot \frac{C_{min}}{C_h} \cdot (\omega_3 - \omega_1)$ $\omega_4 = 0.2035$ "kg water/kg dry air"

$\phi_2 := \frac{\omega_2 \cdot P_2}{(0.622 + \omega_2) \cdot P_{sat}(T_2)}$ $\phi_2 = 0.508$ "converge with initial value"

$\phi_4 := \frac{\omega_4 \cdot P_4}{(0.622 + \omega_4) \cdot P_{sat}(T_4)}$ $\phi_4 = 0.647$ "converge with initial value"

Convert relative humidities to dew point temperatures.

$T_{dp2} := T_{sat}(\phi_2 \cdot P_{sat}(T_2))$ $T_{dp2} = 59.583$ °C $P_{sat}(T_{dp2}) = 0.1959$ bar

$T_{dp3} := T_{sat}(\phi_3 \cdot P_{sat}(T_3))$ $T_{dp3} = 75$ °C

$T_{dp4} := T_{sat}(\phi_4 \cdot P_{sat}(T_4))$ $T_{dp4} = 64.9449$ °C

The water flux at the dry outlet is:

$J_2 := \frac{(\omega_2 - \omega_1) \cdot m'_c}{A}$ $J_2 = 4.5194 \times 10^{-4} \frac{kg}{m^2 \cdot s}$

$m'_{H2O} := (\omega_2 - \omega_1) \cdot m'_c$ $m'_{H2O} = 1.8303 \times 10^{-7}$ kg/s

The dew point approach temperature is then:

DPAT := $T_{dp3} - T_{dp2}$ DPAT = 15.4173 K

Finally, the recommended method to quantify the water transport performance is through the water recovery ratio.

$WRR := \frac{(\omega_2 - \omega_1) \cdot m'_c}{\omega_3 \cdot m'_h}$ WRR = 0.3889